

RESEARCH ARTICLE

Point mutations in Arf1 reveal cooperative effects of the N-terminal extension and myristate for GTPase-activating protein catalytic activity

Eric M. Rosenberg, Jr.  ¹*, Xiaoying Jian  ¹*, Olivier Soubias ², Rebekah A. Jackson  ², Erin Gladu ¹, Emily Andersen ¹, Lothar Eßer ³, Alexander J. Sodt ⁴, Di Xia ³, R. Andrew Byrd  ², Paul A. Randazzo  ¹*

1 Laboratory of Cellular and Molecular Biology, Center for Cancer Research, National Cancer Institute, Bethesda, MD, United States of America, **2** Section of Macromolecular NMR, Center for Structural Biology Laboratory, Center for Cancer Research, National Cancer Institute, Frederick, MD, United States of America, **3** Laboratory of Cell Biology, Center for Cancer Research, National Cancer Institute, Bethesda, Maryland, United States of America, **4** Unit of Membrane Chemical Physics, *Eunice Kennedy Shriver National Institute of Child Health and Human Development*, Bethesda, MD, United States of America

* These authors contributed equally to this work.

* randazzp@mail.nih.gov



OPEN ACCESS

Citation: Rosenberg EM, Jr., Jian X, Soubias O, Jackson RA, Gladu E, Andersen E, et al. (2024) Point mutations in Arf1 reveal cooperative effects of the N-terminal extension and myristate for GTPase-activating protein catalytic activity. PLoS ONE 19(4): e0295103. <https://doi.org/10.1371/journal.pone.0295103>

Editor: Jude M. Przyborski, Justus Liebig Universität Giessen, GERMANY

Received: November 13, 2023

Accepted: March 5, 2024

Published: April 4, 2024

Copyright: This is an open access article, free of all copyright, and may be freely reproduced, distributed, transmitted, modified, built upon, or otherwise used by anyone for any lawful purpose. The work is made available under the [Creative Commons CC0](#) public domain dedication.

Data Availability Statement: The data for all structures used in this paper are freely available to the public through the protein data bank (<https://www.rcsb.org>). Here is the direct link to the PDB with the atomic coordinates: <https://www.rcsb.org/structure/8SDW>, as well as DOI: <https://doi.org/10.2210/pdb8SDW/pdb>. For the diffraction images themselves, the website with instructions on how to download: <https://data.sbggrid.org/dataset/1080/>, and the DOI: <https://doi.org/10.15785/SBGRID/1080>.

Abstract

The ADP-ribosylation factors (Arfs) constitute a family of small GTPases within the Ras superfamily, with a distinguishing structural feature of a hypervariable N-terminal extension of the G domain modified with myristate. Arf proteins, including Arf1, have roles in membrane trafficking and cytoskeletal dynamics. While screening for Arf1:small molecule co-crystals, we serendipitously solved the crystal structure of the non-myristoylated engineered mutation [L8K]Arf1 in complex with a GDP analogue. Like wild-type (WT) non-myristoylated Arf1•GDP, we observed that [L8K]Arf1 exhibited an N-terminal helix that occludes the hydrophobic cavity that is occupied by the myristoyl group in the GDP-bound state of the native protein. However, the helices were offset from one another due to the L8K mutation, with a significant change in position of the hinge region connecting the N-terminus to the G domain. Hypothesizing that the observed effects on behavior of the N-terminus affects interaction with regulatory proteins, we mutated two hydrophobic residues to examine the role of the N-terminal extension for interaction with guanine nucleotide exchange factors (GEFs) and GTPase Activating Proteins (GAPs). Different than previous studies, all mutations were examined in the context of myristoylated Arf. Mutations had little or no effect on spontaneous or GEF-catalyzed guanine nucleotide exchange but did affect interaction with GAPs. [F13A]myrArf1 was less than 1/2500, 1/1500, and 1/200 efficient as substrate for the GAPs ASAP1, ARAP1 and AGAP1; however, [L8A/F13A]myrArf1 was similar to WT myrArf1. Using molecular dynamics simulations, the effect of the mutations on forming alpha helices adjacent to a membrane surface was examined, yet no differences were detected. The results indicate that lipid modifications of GTPases and consequent anchoring to a membrane influences protein function beyond simple membrane localization. Hypothetical mechanisms are discussed.

Funding: This work was supported by the Intramural Research Program of the National Cancer Institute, National Institutes of Health, Department of Health and Human Services (project number BC007365 to P. A. R.). The funders had no role in study design, data collection and analysis, decision to publish, or preparation of the manuscript.

Competing interests: The authors have declared that no competing interests exist.

Introduction

The ADP-ribosylation factor (Arf) family of small GTPases within the Ras superfamily regulate membrane trafficking and cytoskeletal reorganization and are being investigated for roles in cancer progression [1, 2]. Arf function depends on cycling between GDP- and GTP-bound states. Different than other families of GTPases, intrinsic exchange rates and GTPase rates of Arf proteins are slow or negligible, and they therefore depend on guanine nucleotide exchange factors (GEFs) and GTPase-activating proteins (GAPs) for activity [3, 4]. The G domain architecture of Arf proteins is similar to other G proteins, consisting of a P loop, G4 motif, and G5 motif that bind to guanine nucleotides, as well as switch regions I and II (and interswitch region) that are conformationally different depending on the guanine nucleotide bound [5]. Like other small GTPases, Arf proteins have a lipidated hypervariable region (HVR), but different than other small GTPases, the HVR is an N-terminal extension of typically 16 amino acids from the G domain that is co-translationally modified with myristate on the glycine at position 2 [6, 7]. In cells, both the N-terminal extension and the myristate are essential; [$\Delta 17$]Arf1 and [G2A]Arf1 have no detectable activity in yeast or mammalian cells and peptides comprised of the N-terminal extensions of Arf proteins block Arf functions [8, 9]. The possible coupling of the myristate with residues of the N-terminus is understudied and the molecular bases for the requirement of myristate and the N-terminal extension are still being discovered.

The myristate is often considered to function as a membrane anchor, important for confining proteins to specific endomembranes but otherwise not critical for interaction with target proteins [10, 11]. Prior to this report, results examining Arf GAPs appear to be consistent with this hypothesis. [$\Delta 17$]Arf1 is a poor substrate for Arf GAPs [12, 13]. In the context of the full-length non-myristoylated protein, specific residues within the N-terminal extension of Arf1 were found to be critical, including lysines at positions 10, 15, and 16 [13, 14]. The possible interaction of the myristate with the N-terminal extension in determining GAP activity was not pursued beyond an examination of wild-type (WT) Arf1, in which myristate did not affect GAP activity [15, 16]. In the NMR structure of yeast myristoylated Arf•GTP, the myristate was buried in lipid bicelles where it formed significant contacts with the conserved residue leucine 8, a residue not critical for GAP activity (in the context of non-myristoylated protein) [14, 17]. These results were interpreted as consistent with the conclusion that myristate does not have a role in GAP activity.

The possibility that the N-terminal 16 amino acids of Arf and the myristate function in a cooperative way (i.e., causing effects only when both are present) to influence GEF activity has not been examined to our knowledge. Full-length, non-myristoylated Arf1 is a poorer substrate for GEFs than is [$\Delta 17$]Arf1, while full-length myristoylated Arf1 (hereby referred to as “myrArf”) is a better substrate than [$\Delta 17$]Arf1 [18, 19]. The myristate has a clear functional role by itself: integrated structural biology approaches have revealed a role for the myristate in anchoring the transition complex of nucleotide exchange to a hydrophobic surface [20, 21]. Within Arf•GDP, myristate affects the structure of the N-terminal extension: whereas the N-terminal extension forms an alpha helix that occupies a hydrophobic cavity in non-myristoylated Arf•GDP, the myristate occupies the same site in myrArf with a disordered N-terminal extension floating on top, potentially increasing accessibility for the GEF [22, 23]. Thus, based on these limited results, the myristate and N-terminal extensions of Arf proteins might have codependent function.

Here, we solved the crystal structure of the non-myristoylated engineered Arf1 mutant, [L8K]Arf1, bound to a GDP analogue (G3D). This mutant was previously generated to remove the requirement for a membrane surface for GTP/GDP exchange [24]. We found significant differences in the interface between the N-terminus of Arf and the G domain from that

observed with WT Arf1. Although this interface is fortuitous in the non-myristoylated protein, it indicated that single amino acid differences in this part of Arf could influence protein interactions such as with GAPs and, potentially, with GEFs. This result motivated us to reexamine the role of the N-terminus in nucleotide exchange and GAP-dependent GTPase activity, using myristoylated Arf to minimize fortuitous interactions occurring in its absence. We focused on two hydrophobic residues in the N-terminus of Arf1, leucine 8 (L8) and phenylalanine 13 (F13). Although mutating L8 and F13 had little or no effect on spontaneous or catalyzed nucleotide exchange, mutating F13 affected GAP-induced GTP hydrolysis by several orders of magnitude. The effect of mutating F13 was reversed by simultaneously mutating L8. In previous studies, mutations of the same residues in non-myristoylated Arf1 had little or no effect on GAP-induced GTP hydrolysis [14]. Molecular dynamics (MD) simulations on myristoylated N-terminal peptides suggested that the mutations do not affect peptide secondary structure, indicating that there is yet another undefined mechanism by which these mutations affect Arf GAP activity. Together, our results reveal cooperative function of the myristate and the N-terminus in GAP-dependent regulation of Arf, which might extrapolate to Arf effectors. Furthermore, our results are consistent with the idea that the N-terminal amino acids of Arf have a critical role in Arf GAP but not Arf GEF activity.

Results

The crystal structure of non-myristoylated [L8K]Arf1 in complex with a GDP analogue exhibits an unexpected N-terminal shift

While conducting crystal screens for small molecules that bind to Arf proteins [25], we serendipitously crystallized non-myristoylated [L8K]Arf1 in complex with a GDP analogue (namely guanosine-3'-monophosphate-5'-diphosphate or G3D, discussed below). These crystals formed regardless of the presence of the small molecule ligands, and we therefore solved the structure of an *apo* crystal to 1.75 Å in order to ensure that no features of the data were present as a result of binding to these small molecules. Crystallographic statistics are shown in [Table 1](#), and the overall structure of [L8K]Arf1•G3D (PDB accession code 8SDW) is shown in [Fig 1A](#). There is only a single monomer of [L8K]Arf1 in the crystal asymmetric unit, with residues 6–180 visible in the structure; in addition to residues 2–5, part of switch II (residues 70–74) was too disordered to be modeled. The macromolecule is clearly bound to a magnesium ion as well as a guanine nucleotide that was initially thought to be GDP, but was later determined to be G3D, a GDP molecule with a phosphate in the 3' position ([S1A Fig](#)). G3D has been found in other structures of small GTPases including Arf [21, 26–28], Arf-like (Arl) [29], and Rab [30] structures, as well as a presumed nucleoside kinase, yorR [31], although its significance in these structures has yet to be determined and is likely an artifact of overexpression in *E. coli*. Although outside of the scope of this work, G3D has a known role in the bacterial stringent response, which occurs when bacteria are under conditions of amino acid starvation during growth [32–34].

The crystal structure of [L8K]Arf1 is largely similar to that of full-length non-myristoylated WT Arf1 in complex with GDP (PDB accession code 1HUR [22]) with only minor structural rearrangements ([Fig 1B and 1C](#)). The most striking difference between the WT and [L8K] structures is in the positioning of their N-terminal residues; while both structures exhibit amphipathic helices that occlude the hydrophobic cavity where the myristoyl group is typically found in the native protein (see next section), the helices are offset by 6.5 Å (L8_{Cα} to K8_{Cα}). Further, the hinge region between the N-terminal helix and β1 is approximately 7.1 Å (K16_{Cα-Cα}) more extended in the WT structure than in the [L8K] structure ([Fig 1C](#)). Calculating the RMSD of a monomer from 1HUR with the [L8K]Arf1 monomer highlights the large structural

Table 1. [L8K]Arf1•G3D crystal data collection and refinement statistics.

	[L8K]Arf1•G3D (PDB: 8SDW)
Data collection	
Space group	P2 ₁ 2 ₁ 2 ₁
Cell dimensions	
<i>a, b, c</i> (Å)	41.65, 55.02, 78.47
α, β, γ (°)	90.0, 90.0, 90.0
Resolution (Å)	50.00–1.75 (1.78–1.75)
<i>R</i> p.i.m.	0.025 (0.078)
CC _{1/2}	0.996 (0.976)
<i>I</i> / σ <i>I</i>	27.10 (9.33)
Completeness (%)	98.7 (89.8)
Redundancy	6.2 (5.8)
Refinement	
Resolution (Å)	39.24–1.75 (1.81–1.75)
No. reflections	18523
<i>R</i> _{work} / <i>R</i> _{free}	0.19/0.21
No. atoms	1651
Protein	1322
Ligand/ion	33
Water	296
<i>B</i> -factors	
Protein	20.4
Ligand/ion	17.1
Water	30.1
R.m.s. deviations	
Bond lengths (Å)	0.005
Bond angles (°)	1.01

The data set was obtained from a single crystal, and the resulting data collection and refinement statistics are shown. Values in parentheses are for the highest resolution shell.

<https://doi.org/10.1371/journal.pone.0295103.t001>

changes apparent as a result of the N-terminal shift. When comparing only residues 18–180, the RMSD values between the structures are 0.82 and 0.81 Å (between either α -carbons and backbone atoms); by including residues 6–17 in the analysis, the RMSD values are 1.95 and 1.98 Å. Another difference between the structures is the interswitch region, which in the [L8K] structure moves approximately 2.4 Å (based on averaged $\text{C}\alpha$ - $\text{C}\alpha$ distances of K59 and N60) towards the cavity compared to the WT structure (Fig 1C). While we do not interpret the changes in the N-terminal helix and hinge/interswitch regions of [L8K]Arf1 to be a result of crystal contacts (nor can crystal contacts easily explain the positioning of the N-terminal helix in the WT structure, given that there are two monomers in the asymmetric unit with non-identical crystal contacts [22]), we note that the interswitch region is adjacent to a symmetry mate in the crystal lattice, and therefore some of the observed changes in these regions of the protein may be an artifact of crystallization rather than a feature brought about the L8K mutation (S1B Fig). The interface in this region is complex, with both intramolecular and intermolecular interactions being observed. Specifically, we note intramolecular hydrogen bonds that are made between N60 to G14 and K16 (S1B Fig), as well as several hydrophobic interactions between the N-terminal extension and the G domain hydrophobic cavity (discussed in next section). Intermolecular contacts are formed between the interswitch residues Y58 and K59,

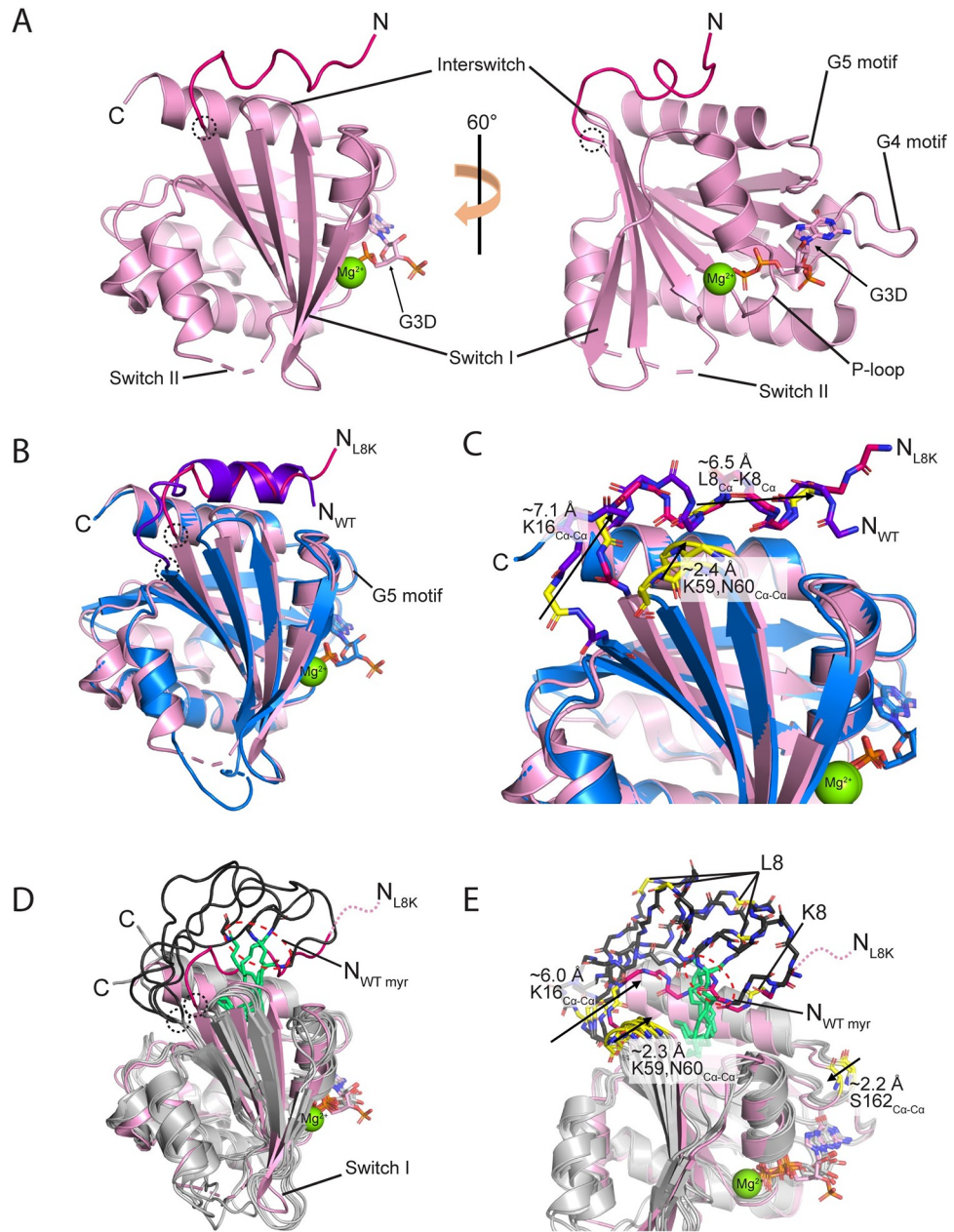


Fig 1. Comparison of [L8K]Arf1 crystal structure with human and yeast Arf1 structures. (A) Crystal structure of [L8K]Arf1 in complex with guanosine-3'-monophosphate-5'-diphosphate (G3D). N- and C-termini, G domain motifs, and magnesium ion are labeled. Part of switch II could not be modeled and is depicted with dashed lines. The G domain is shown in pink and the N-terminal extension in hot pink; a dotted circle marks the point at which the N-terminus ends and the G domain begins. (B) Overall superimposition of [L8K]Arf1•G3D (pink and hot pink) and non-myristoylated WT Arf1•GDP (blue and purple, PDB: 1HUR [22]) crystal structures. Differences in the positioning of the N-terminal residues are labeled. N-terminal extension/G domain demarcation points are indicated as in (A). (C) Structural differences between [L8K]Arf1•G3D and non-myristoylated WT Arf1•GDP. Movements of residues within the N-terminal extension, the hinge region connecting the N-terminus and G domain, and the interswitch region in the [L8K] structure compared to WT are depicted with arrows. Backbone atoms of residues used for measurements are colored yellow, and distances of α -carbon movements are shown. Structures are colored as described in (B). (D) Overall superimposition of the [L8K]Arf1•G3D crystal structure (pink and hot pink) and the *S. cerevisiae* WT myrArf1•GDP NMR structure (grey and black, PDB: 2K5U [23]). Differences between the N-termini are also highlighted: residues 2–5 in the [L8K] structure are disordered and could not be modeled, but their relative positioning as an extension of the modeled N-terminal residues are depicted with a dashed line. The positioning of the N-terminal G2 residue that is covalently modified with the myristoyl moiety in the yeast myrArf1 structure is shown

with a red dashed oval, and the myristate moiety is shown in lime green. Note that four out of the sixteen NMR states of the yeast myrArf1 structure are depicted. N-terminal extension/G domain demarcation points are indicated as in (A). (E) Structural differences between [L8K]Arf1•G3D and yeast WT myrArf1•GDP. Movements of the hinge region connecting the N-terminus and G domain, the interswitch region, as well as G5 motif in the [L8K] structure compared to yeast myrArf1 are depicted with arrows. Backbone atoms of residues used for measurements are colored yellow, and distances of α -carbon movements are shown. Differences in the positioning of the N-terminal residues and coloring of structures are as described in (D).

<https://doi.org/10.1371/journal.pone.0295103.g001>

which help to coordinate the phosphates on a G3D of a symmetry mate. Additional intermolecular crystal contacts are formed between part of the N-terminal extension to a symmetry mate, namely K10 and the backbone of K15 that form a salt bridge with the 3' phosphate moiety in G3D and a hydrogen bond with Y35 in $\alpha 1$ (S1B Fig). The L8K mutation itself is near D141 of a different symmetry mate, a residue on an α -helix in the G domain, but is not optimally positioned for forming a salt bridge (S1C Fig).

Although the structure of human myrArf1•GDP has not been determined, the NMR structure of *S. cerevisiae* myrArf1•GDP is available (PDB accession code 2K5U [17]). *S. cerevisiae* and human Arf1 are the same length (181 residues) and share 77% identity/88% similarity, with the differences scattered throughout their primary structure. Their N-terminal extensions are also the same length, namely 16 amino acids (residues 2–17) after processing. The yeast myrArf1 structure highlights the fact that the N-terminal extension of Arf1 is typically disordered in the GDP-bound state, with the myristoyl moiety inserting into a hydrophobic cavity between the interswitch region and the C-terminal alpha helix (Fig 1D and 1E). By comparing the yeast myrArf1•GDP and [L8K]Arf1•G3D structures, it is apparent that the most obvious differences lie in the positioning of their N-terminal extensions; in addition, the hinge region between the N-terminal extension and the first beta strand is approximately 6.0 Å (K16_{C α -C α) more extended in the yeast myrArf1 structure than in the [L8K]Arf1 structure, similar to WT non-myrArf1 (Fig 1C and 1E). Like the changes noted between the positioning of the interswitch regions in non-myristoylated WT Arf1•GDP and [L8K]Arf1•G3D, we observe that the interswitch of [L8K]Arf1•G3D appears to move inward approximately 2.3 Å (based on averaged C α -C α distances of K59 and N60); however, the multiple states of the interswitch in the NMR structure indicates that the interswitch is relatively flexible in general (Fig 1D and 1E). [L8K]Arf1•G3D also shows a ~2.2 Å (S162_{C α -C α) inward movement of the G5 motif compared to yeast myrArf1•GDP (Fig 1E). The inward movement of the G5 motif may be mediated by crystal contacts (S1C Fig). Alternatively, movement of the G5 motif may be a difference between yeast and human Arf1 as the G5 motif is the same position in the human WT non-myrArf1 structure as it is in the human [L8K]Arf1 structure (Fig 1B). However, the human structures were determined with protein that was not myristoylated, and therefore the G5 movement might be driven by the myristate. A similar change between the human structures (non-myristoylated) and the yeast structure (myristoylated) is in the positioning of switch I (Fig 1B and 1D).}}

When comparing all three Arf1 GDP-state structures (i.e., yeast myrArf1, human non-myristoylated WT Arf1, and [L8K]Arf1), it is not only the positioning of their N-terminal extensions that differ (Fig 1), but the hinge regions between the G domain and the N-terminus (S1D Fig). In addition to the C α -C α movements of K16 already described (with movements of ~7.1 and ~6.0 Å, Fig 1C and 1E), K16 is offset by approximately 7 Å when comparing non-myristoylated WT Arf1 and yeast myrArf1 (S1D Fig). Altogether, the structures indicate that the N-terminal end of $\beta 1$ in the G domain as well as the hinge region are flexible, and are therefore able to accommodate the rearrangements requisite for the positioning of the N-terminal extension in all three structures.

The hydrophobic cavity of Arf1•GDP is occupied by either a myristoyl moiety in myrArf1 or the hydrophobic residues in the N-terminal extension of non-myristoylated Arf1

Examination of the location of the L8K mutation revealed that this residue, while located inside the hydrophobic cavity in the non-myristoylated WT structure as L8, is instead found outside of the hydrophobic cavity when mutated to lysine (Fig 2). Interestingly, the N-terminal shift as a result of the L8K mutation is also achieved by redundancies in the N-terminal sequence of Arf1—while the hydrophobic cavity in the WT structure is filled by residues F5, L8, F9, L12, and partly M18, the cavity in the [L8K] structure is instead filled by F9, L12, F13, and M18 to a greater degree (Fig 2A–2C and Table 2). Indeed, the amino acid side chain positions of I4, F5, L8, and F9 are almost identical to the side chain positions of K8, F9, L12, and F13 in the [L8K] structure (Fig 2A and Table 2). L12 in the WT structure is the only residue in the cavity that is not replaced by an identical amino acid in the [L8K] structure; instead, M18 shifts over by more than 3 Å in order to fill in the cavity (Fig 2A and Table 2). Similarly, the movement of the inter-switch region in the [L8K] structure shrinks the hydrophobic cavity by approximately 10% compared to the non-myristoylated WT structure, potentially minimizing the free energy of the protein by increasing hydrophobic contacts with the buried N-terminal extension residues. Indeed, the surface area of the N-terminal extension residues contacting the G domain hydrophobic cavity drops by approximately 11–26% in the L8K structure compared to the non-myristoylated WT structure, supporting this interpretation. The ordered positions of these N-terminal residues are in stark contrast to their positions in yeast myrArf1•GDP, in which they are exposed to solvent and only the myristate moiety occupies the hydrophobic cavity (Fig 2D).

Mutations in the N-terminal extension of Arf1 may have differing effects dependent on whether Arf1 is myristoylated

The association of the N-terminus of Arf with the G domain occurs in non-myristoylated Arf, and is therefore a fortuitous and non-physiological association. Nevertheless, it represents a specific interface that is significantly altered by a single amino acid change. Other, physiologically relevant binding sites, for example in Arf GAPs, might similarly be affected. We also considered that the myristate might influence the binding, guiding the peptide towards physiological sites or preventing binding to irrelevant sites. Effects of mutating the N-terminus of Arf on GAP activity have been studied only in the context of the non-myristoylated protein, motivating us to reexamine some of the mutants in the context of myristoylated Arf. We are not aware of an examination of the role of the N-terminus in GEF activity, despite the large conformational shift of the N-terminus that accompanies nucleotide exchange. To address this gap in the literature, we also examined the effect of mutating the N-terminus of Arf on GEF activity. We focused on two residues. L8 contributes to membrane association as seen in the yeast myrArf1•GTP NMR structure (Fig 3A); interestingly, L8 also forms hydrophobic interactions with the distal end of the myristoyl moiety in this structure (Fig 3B), in contrast to our more recent analyses of human myrArf1•GTP bound to nanodiscs [35], leading us to reason that changes in L8 might alter activities in the context of the myristoylated protein. Here, we also examine the effect of mutating F13, which is surface-exposed in WT human non-myristoylated Arf1 but is buried into the hydrophobic cavity in [L8K]Arf1. In yeast myrArf•GDP, F13 is in a disordered loop exposed to solvent in yeast myrArf1 (Fig 2B–2D) and in yeast myrArf•GTP is adjacent to the membrane (Fig 3A), which does not exclude a role for direct interaction with either a GEF or a GAP. These residues were also chosen to be examined because both are among the most well-conserved in Arf N-termini, with only Arf6 and Arf3 exhibiting different residues at these positions (Fig 3C).

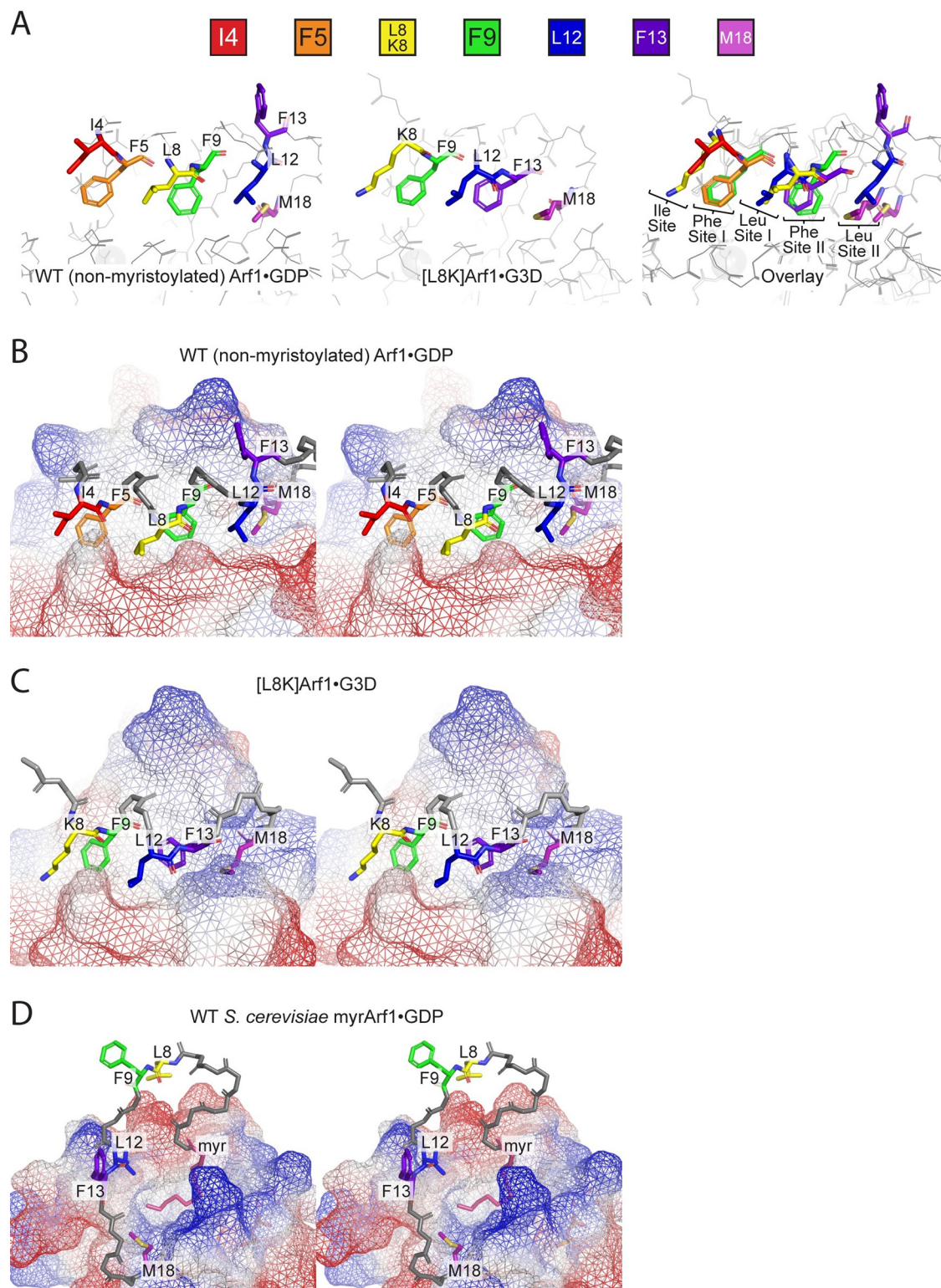


Fig 2. Examination of how the Arf1 G domain hydrophobic cavity is occupied by the N-terminal extension in Arf1 structures. (A) Comparison of the positions of residues within the N-terminal extensions of non-myristoylated WT Arf1•GDP (left) and [L8K] Arf1•G3D (middle). An overlay of the two structures is shown on the right, with arbitrary labels for the positions of the amino acid side chains shown to aid the reader in interpretation; see also Table 2. For both structures, the amino acids that fill the hydrophobic cavity in the G domain are labeled and shown as colored sticks (key on top). (B) Stereoscopic view of the non-myristoylated WT

Arf1•GDP N-terminal extension. The surface of the G domain is depicted in a mesh, with blue and red indicating positive and negative surface charges. Amino acids that fill the hydrophobic cavity are colored as described in (A). (C) Stereoscopic view of the [L8K]Arf1•G3D N-terminal extension. Colors of amino acids are as described in (A), and other features as described in (B). (D) Stereoscopic view of a single pose of the *S. cerevisiae* WT myrArf1•GDP N-terminal extension. Note that this view is from a different angle than those shown in (B) and (C), for clarity. The myristoyl moiety is shown in pink, and colors of amino acids that are conserved with human Arf1 (i.e., L8, F9, L12, F13, and M18, see Fig 3C) are as described in (A). Other features are as described in (B).

<https://doi.org/10.1371/journal.pone.0295103.g002>

N-terminal mutations in myristoylated Arf1 affect neither spontaneous exchange nor activity of the Arf GEF Brag2

The N-terminal extension of Arf undergoes a positional and conformational change on exchange of nucleotide and has an established role in nucleotide exchange [21]. The contribution of individual residues within the N-terminus, however, has not been examined, particularly in the context of myristoylated Arf. Here, we examined the effects of L8 and F13 on spontaneous exchange, which was accelerated by buffering Mg²⁺ to 1–10 μM using EDTA. Specifically, we examined the Arf1 mutants L8K, L8A, F13A, as well as the double mutant L8A/F13A. Large unilamellar vesicles (LUVs) were included in the assay to accommodate the myristate. Compared with WT myrArf1, the rate and extent of binding GTPγS were within two-fold of one another, which, given the errors, were not significantly different (S2 Fig). We concluded that L8 and F13 do not significantly affect spontaneous exchange in myrArf1.

Similarly, little or no change in GEF-catalyzed exchange among the mutants was detected. In our experiments, Brag2, a phosphoinositide-dependent GEF [36], was used as a model GEF. The Sec7-PH domain tandem of Brag2 (Fig 4A, top) was titrated into a reaction mixture containing [³⁵S]GTPγS, the indicated myrArf1 mutant, and LUVs containing phosphatidylinositol 4,5-bisphosphate (PIP2). The amount of Brag2 necessary for 50% of maximum observed nucleotide exchange (C₅₀) was determined, which is inversely related to enzymatic power. The C₅₀ of Brag2 for WT myrArf1 was 1.9 nM, and all the mutants were within ~2-fold of that value (Fig 4 and Table 3). The C₅₀ using [F13A]myrArf1 was about 2-fold greater than for WT myrArf1 or myrArf1 with mutations in L8, (p < 0.01, Fig 4 and Table 3). Thus, despite the previously documented changes in the N-terminal extension of Arf1 on switching between GTP- and GDP-bound forms of Arf, neither L8 nor F13 has a dominant effect.

Table 2. Relative positions of N-terminal extension residues within the non-myristoylated WT Arf1•GDP and [L8K]Arf1•G3D crystal structures.

Residue	In non-myristoylated WT Arf1•GDP structure (PDB: 1HUR)	In non-myristoylated [L8K]Arf1•G3D structure (PDB: 8SDW)
I4	I4 occupies “Isoleucine Site”	No visible density
F5	Occupies “Phenylalanine Site I”	No visible density
L8/K8	L8 occupies “Leucine Site I”	K8 overlays with position of I4 in WT structure, thereby occupying “Isoleucine Site”
F9	Occupies “Phenylalanine Site II”	Overlays with position of F5 in WT structure, thereby occupying “Phenylalanine Site I”
L12	Occupies “Leucine Site II”	Overlays with position of L8 in WT structure, thereby occupying “Leucine Site I”
F13	Exposed to solvent in hinge region	Overlays with position of F9 in WT structure, thereby occupying “Phenylalanine Site II”
M18	Partly filling hydrophobic cavity	Filling hydrophobic cavity more than in WT structure by occupying “Leucine Site II”

See also Fig 2. Note that the “Phenylalanine/Leucine Site I/II” distinctions are arbitrary and are only intended to aid the reader in interpreting differences between the structures.

<https://doi.org/10.1371/journal.pone.0295103.t002>

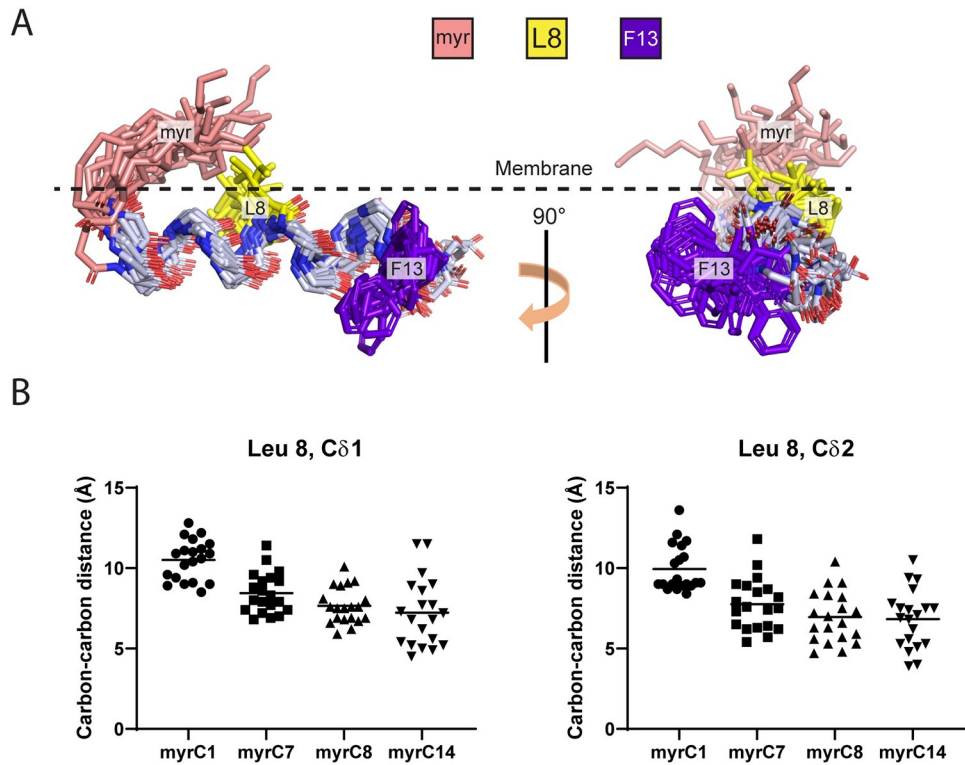


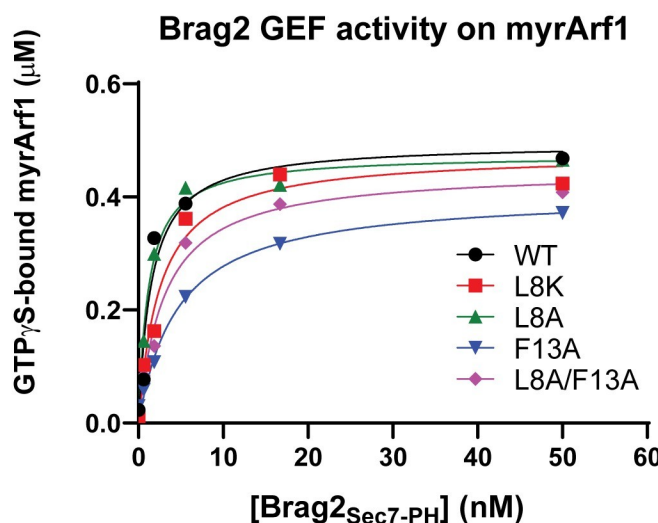
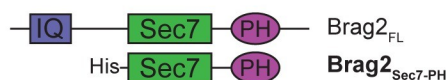
Fig 3. Positioning and conservation of residues L8 and F13 in Arf N-terminal extensions. (A) NMR structure of the N-terminal extension of *S. cerevisiae* WT myrArf1•GTP bound to bicelles (PDB: 2KSQ [17]). Note that all NMR states of the structure are depicted. The rough positioning of the outer layer of the phospholipid membrane is shown as a dashed line, and the myristate moiety, L8, and F13 are labeled and shown as colored sticks (key on top). (B) Carbon-carbon distances between the indicated carbons from the myristoyl moiety and L8 in yeast WT myrArf1•GTP. Distances were obtained from each of the 20 states within the NMR structure. (C) Alignments of the N-terminal extension primary sequences of *S. cerevisiae* Arf1 as well as human Arf1, Arf3, Arf4, Arf5, and Arf6. Amino acids that are identical are marked with an asterisk, whereas those with low and high similarity are marked with a period or a colon. Colors of amino acids that align with yeast L8 and F13 are the same as in (A). The N-terminal extensions are represented by the horizontal line on top. Swiss-Prot identifiers are shown on the left, and amino acid positions on the right.

<https://doi.org/10.1371/journal.pone.0295103.g003>

N-terminal mutations in myrArf1 affect activity with Arf GAPs

We have previously reported a mutational analysis of the effect of the N-terminus on interaction with Arf GAPs [14]. In those studies, neither L8 nor F13 were found to have a significant effect; however, they were examined in the context of non-myristoylated Arf1. Because of the possibility that the presence of the myristate could affect binding of the N-terminus to proteins, we tested each of the mutants as a substrate for the catalytic fragment of the Arf GAP ASAP1 (Fig 5A and 5B). ASAP1 was titrated into a reaction mixture containing the myrArf1 proteins bound to [α^{32} P]GTP and LUVs containing the activating phosphoinositide PIP2.

A



B

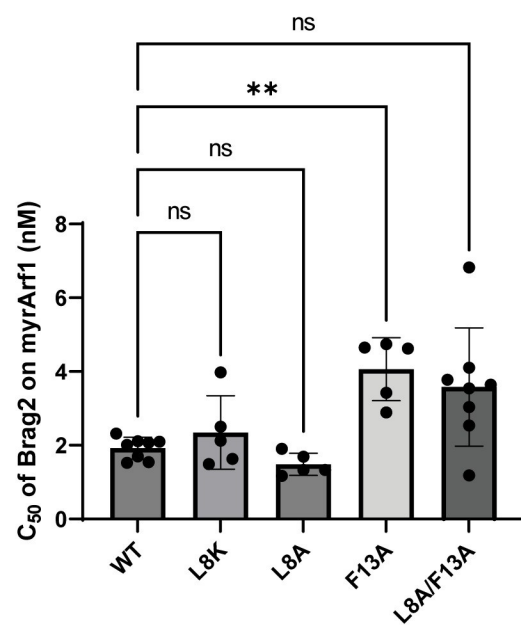


Fig 4. Brag2 GEF activity using the indicated myrArf1-GDP as substrate. (A) A representative example of a GEF assay from multiple experiments. For these assays, the His-tagged Brag2_{Sec7-PH} construct (see top for comparison with full-length [FL] construct) was titrated into a reaction with [³⁵S]GTP_γS, LUVs, and 0.5 μM myrArf1 constructs. After a fixed period of time, the fraction of myrArf1 bound to [³⁵S]GTP_γS was measured. IQ, IQ motif; Sec7, Sec7 catalytic domain; PH, Pleckstrin Homology domain. (B) Summary of Brag2 GEF activity assays using the indicated myrArf1-GDP as substrate. C₅₀ values (the concentration of Brag2_{Sec7-PH} required to achieve 50% of maximum loading of the myrArf1 with GTP_γS) from each independent experiment are shown. Error bars represent standard deviation. ns, not significant; **, p < 0.01 via one-way ANOVA with repeated measures (and mixed effects) and Dunnett's multiple comparisons test against WT.

<https://doi.org/10.1371/journal.pone.0295103.g004>

Reactions were stopped after a fixed time and the conversion of [α^{32} P]GTP to [α^{32} P]GDP was measured. The amount of GAP required to achieve 50% hydrolysis in the fixed time (C₅₀) was estimated and, similar to the GEF reactions, is inversely proportional to enzymatic power.

Mutation of L8 alone to either alanine or lysine had little effect on ASAP1 GAP activity, while the F13A mutation increased the C₅₀ ~2700-fold over WT myrArf1 (Fig 5A, 5B and

Table 3. Summary of Arf GEF and GAP assays using myrArf1 constructs.

myrArf1 protein	GEF assays		GAP assays					
	Brag2 _{Sec7-PH}		ASAP1 _{PZA}		AGAP1 _{FL}		ARAP1 _{PPZA}	
	C ₅₀ (nM)	Fold change	C ₅₀ (nM)	Fold change	C ₅₀ (nM)	Fold change	C ₅₀ (nM)	Fold change
WT	1.9 ± 0.35 (5)	1	0.79 ± 0.26 (5)	1	1.6 ± 0.51 (3)	1	0.14 ± 0.015 (3)	1
L8K	2.3 ± 1.0 (5)	1.2	0.84 ± 0.33 (6)	1.1	NT		NT	
L8A	1.5 ± 0.30 (5)	0.79	0.84 ± 0.18 (5)	1.1	NT		NT	
F13A	4.1 ± 0.85** (5)	2.2	2100 ± 170**** (4)	2700	340 ± 72**** (3)	210	210 ± 31**** (3)	1500
L8A/F13A	3.4 ± 2.1 (5)	1.8	0.70 ± 0.11 (4)	0.89	NT		NT	

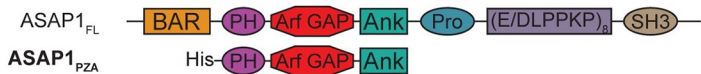
The amount of each enzyme needed to cause 50% maximum exchange (GEFs) or GTP hydrolysis (GAPs) in nanomolar (C₅₀ values) is shown, as well as fold change over WT myrArf1. Numbers in parentheses indicate the number of times the experiment was performed. NT, not tested; significance values are against WT myrArf1

**, p < 0.01

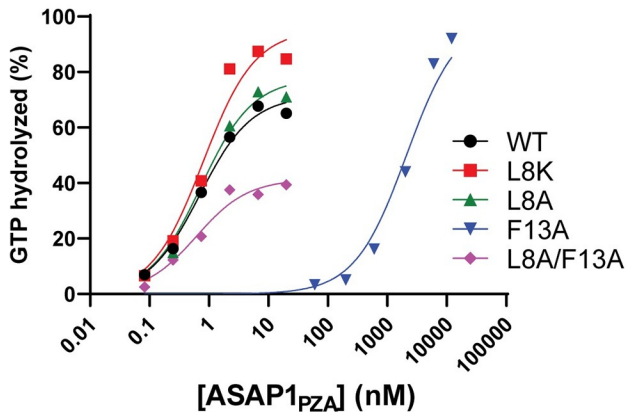
****, p < 0.0001.

<https://doi.org/10.1371/journal.pone.0295103.t003>

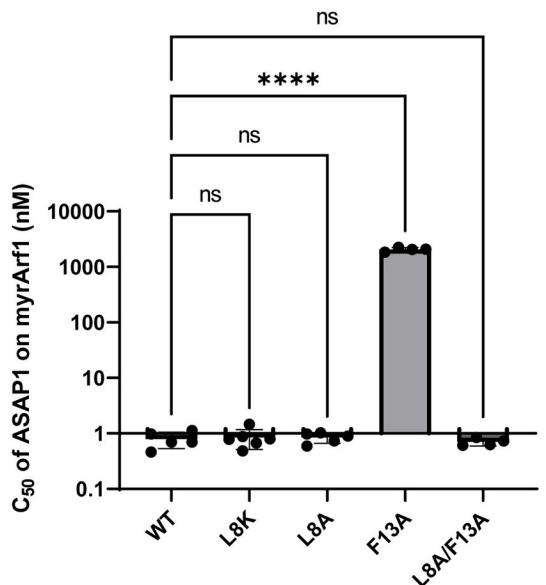
A



ASAP1 GAP activity on myrArf1



B



C

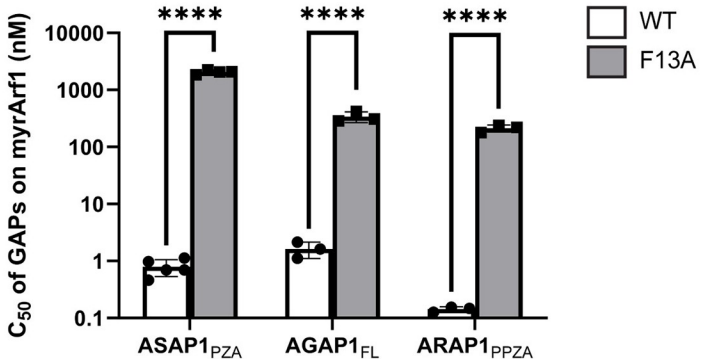
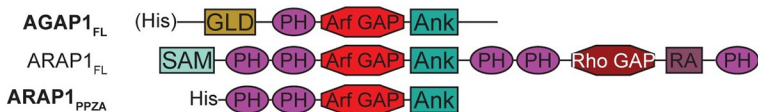


Fig 5. Arf GAP activity using the indicated Arf GAP enzymes and myrArf1•GTP as substrate. (A) ASAP1 GAP activity using the indicated myrArf1•GTP as substrate. For these assays, the His-tagged ASAP1_{PZA} construct (see top for comparison with full-length [FL] construct) was titrated into a reaction with myrArf1 constructs bound to [α^{32} P]GTP on an LUV surface. After a fixed period of time, the ratio of [α^{32} P]GDP and [α^{32} P]GTP bound to myrArf1 was measured. Data shown are a representative example from multiple experiments. BAR, Bin/Amphiphysin/Rvs domain; PH, Pleckstrin Homology domain; Arf GAP, Arf GAP catalytic domain; Ank, Ankyrin repeats; Pro, Proline rich region; E/DLPPKP, E/DLPPKP repeat region; SH3, Src Homology 3 domain. (B) Summary of ASAP1 GAP activity assays using the indicated myrArf1•GTP as substrate. C₅₀ values (the concentration of ASAP1_{PZA} required to achieve 50% of maximum GTP hydrolysis) from each independent experiment are shown. Error bars represent standard deviation. ns, not significant; ****, p < 0.0001 as determined via ordinary one-way ANOVA with Dunnett's multiple comparisons test against WT. Note that while non-transformed data is shown, ANOVA was performed on log₁₀ transformed data in order to satisfy the assumption of equal variances, and the significance using transformed data is displayed. (C) Summary of GAP activity assays of His-tagged proteins ASAP1_{PZA}, full-length (FL) AGAP1, and ARAP1_{PPZA} using WT or [F13A]myrArf1•GTP as substrates. Assays were conducted as described in (A). Error bars represent standard deviation. ****, p < 0.0001 as determined via ordinary two-way ANOVA with Šídák's multiple comparisons test against WT. Note that while non-transformed data is shown, ANOVA was performed on log₁₀ transformed data in order to satisfy the assumption of equal variances, and the significance using transformed data is displayed. GLD, GTP-binding protein-like domain; SAM, sterile- α motif; Rho GAP, Rho GAP catalytic domain; RA, Ras-associating domain. All other protein regions are as described in (A)."

<https://doi.org/10.1371/journal.pone.0295103.g005>

[Table 3](#)). The effect of the F13A mutation on the C₅₀ was reversed by simultaneously including the L8A mutation, although the maximum fraction of GTP hydrolyzed was diminished compared to WT myrArf1 ([Fig 5A, 5B](#) and [Table 3](#); see also [S1 Text](#) and [S3 Fig](#), and relevant citation [37]). To extend our analyses, we examined [F13A]myrArf1 as a substrate for two additional Arf GAP subtypes, AGAP1 and ARAP1 ([Fig 5C](#), top). For these reactions, the activating phospholipids were either PIP2 (AGAP1) or phosphatidylinositol 3,4,5-trisphosphate (PIP3, for ARAP1) [38, 39]. The C₅₀ values of AGAP1 and ARAP1 using [F13A]myrArf1 as a substrate were >200- and ~1500-fold greater than for WT myrArf1 ([Fig 5C](#) and [Table 3](#)). Given that non-myristoylated [F13A]Arf1 was previously observed to have little or no effect on ASAP1 C₅₀ values compared to non-myristoylated WT Arf1 [14], the results reveal the importance of the myristate in determining function of the N-terminus.

Molecular dynamics simulations suggest that a change of phenylalanine 13 to alanine does not affect interaction with the lipid bilayer

We considered the hypothesis that mutations in the N-terminal extension alter its interaction with the membrane in the GTP-bound state. We performed μ s long molecular dynamic (MD) simulations of the WT myristoylated N-terminal extension (residues 2–17) and compared results to peptides carrying single point (L8A, L8K, F13A) or double point (L8A/F13A) mutations. Initially, peptides with residues 2–13 in alpha helical form and residues 14–17 in unstructured form were placed in the membrane following previous observations made by our group [35]. Except for the L8K mutant, no helical kink or bending of the peptide was observed for the WT peptide and its alanine mutants. The peptides were located on average 6.5 ± 3.5 Å below the phosphate plane during the remainder of the simulation, with the long axis of the alpha helical segment roughly perpendicular to the bilayer normal ([Fig 6A and 6B](#)) in good agreement with results obtained for myrArf1•GTP at the membrane [35]. The hydrophobic face of the peptides points toward the bilayer core, and interactions of charged residues with lipid headgroups stabilize the peptide position ([S4A Fig](#)). Alanine mutations did not affect the orientation and dynamics of the myristoyl acyl chain which extends into the lipid matrix, only forming transient contacts with the peptide. On the contrary, introduction of a lysine residue in position 8 drastically changed how peptides interact with the bilayer ([S4 Fig](#)). On average, the orientation and depth of insertion of L8K mutant peptides are less stable along the trajectory. In addition, out of four replicas, one peptide completely loses its alpha helical structure and relocates closer to the lipid headgroup. Overall, despite exhibiting a large shift in GAP C₅₀ values, we did not detect a difference in the myristoylated peptides caused by the F13A mutation, suggesting that another, as of yet to be defined, mechanism renders [F13A]myrArf1 a poor substrate for Arf GAPs.

Discussion

Ras superfamily GTPases are commonly modified in HVRs with lipid moieties, which anchor the proteins to endomembranes. Arf GTPases, part of a subfamily of the Ras superfamily, have an N-terminal extension from the G domain that is cotranslationally and irreversibly myristoylated [6, 40]. The myristate acts, at a minimum, as a membrane anchor; however, the potential function of the myristoylated N-terminal extension of Arf in protein-protein interactions, the molecular bases for its effects on GAP- and GEF-catalyzed transitions, and interdependence of the myristate with other functions of the N-terminus are understudied. Here, by examining the effect of mutating two hydrophobic residues within the N-terminal extension of myrArf1, we discovered a codependence of the myristate and N-terminal extension of Arf on Arf GAP activity.

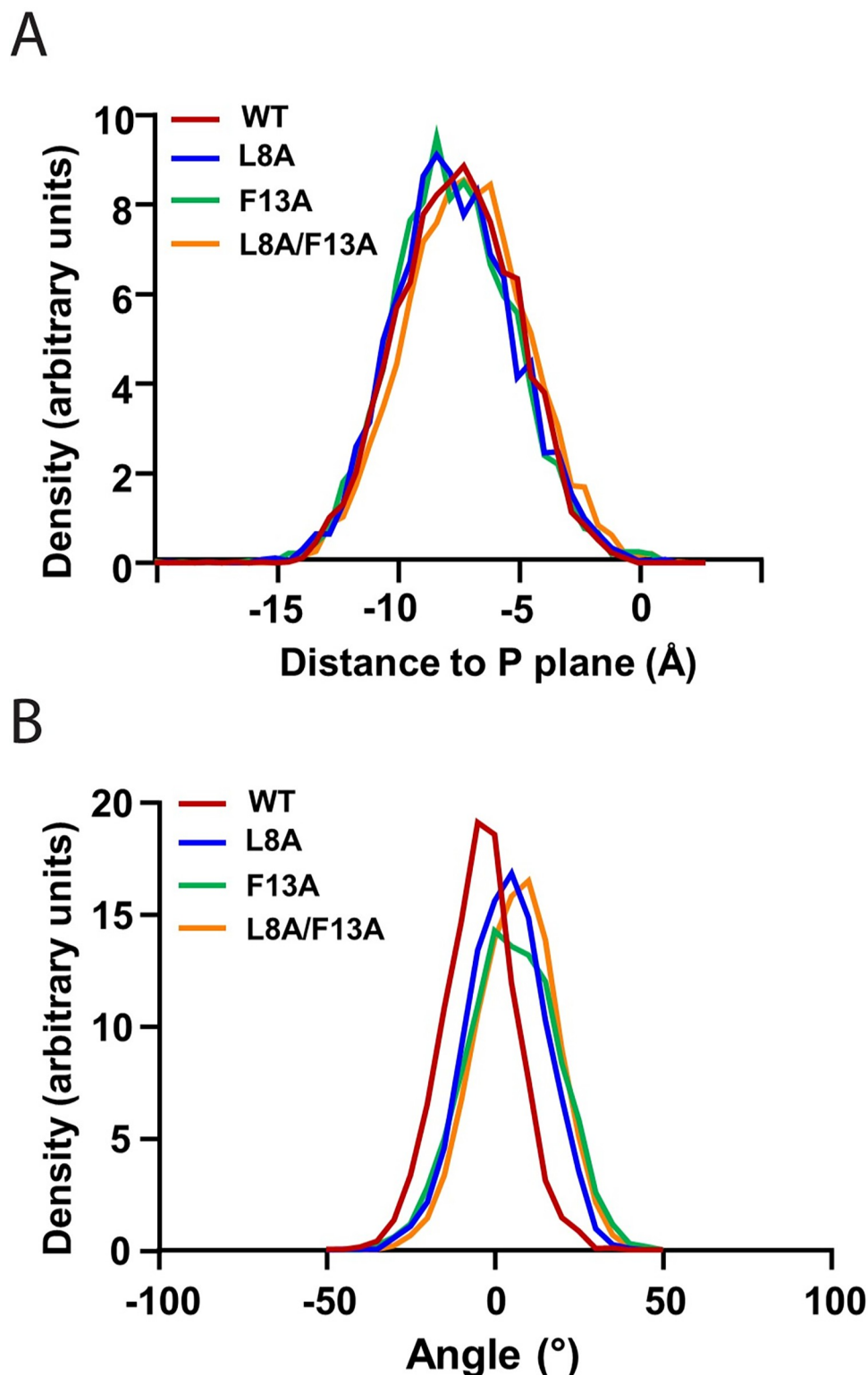


Fig 6. Statistics of myrArf1 N-terminal peptide interaction with membrane from MD simulations. (A) Insertion depth of WT myrArf1 N-terminal peptide and its mutants. The location of peptides was stable along the trajectory with average depth of $-6.8 \pm 2.1 \text{ \AA}$, $-6.7 \pm 2.2 \text{ \AA}$, $-6.9 \pm 2.1 \text{ \AA}$, and $-6.1 \pm 2.2 \text{ \AA}$ relative to the average location of the monolayer phosphate plane for WT, L8A, F13A, and L8A/F13A myrArf1 N-terminal peptides. (B) Average orientation of WT myrArf1 N-terminal peptide and its mutants with respect to the membrane plane. A tilt angle of zero means

that the helical axis is parallel to the membrane surface. A negative tilt angle means the peptide is tilted such that the N-terminus is lower than the C-terminus on the z-axis (membrane normal).

<https://doi.org/10.1371/journal.pone.0295103.g006>

Our results raise questions about the function of the N-terminal myristate of Arf that may go beyond membrane anchoring. The myristate in Arf proteins is distinguished from the lipid modifications of other Ras superfamily members in that it, together with the N-terminal 16 amino acids of Arf, is considered a third switch region that changes conformation and orientation when Arf exchanges GDP for GTP [7]. A comparison of the GDP- and GTP-bound yeast myrArf1 structures provides a clear illustration. In yeast myrArf1•GDP, the myristate lies in a hydrophobic cavity in the G domain upon which the N-terminus floats as an unstructured peptide [23]; in the GTP-bound state, the cavity is vacated, with the myristate embedding in the membrane and the N-terminus forming an alpha helix [17]. The myristate also has a structural function in Arf•GDP. Without myristate, the N-terminal extension folds into an amphipathic helix that occupies the hydrophobic cavity normally occupied by myristate [22]. The myristate, therefore, is not only embedded in the GDP-bound protein but is also important to the structure of the N-terminus of Arf in this state. From another perspective, the myristate prevents the binding of the N-terminus to a site within Arf, leading to the speculation that the myristate can influence the interaction of the N-terminus of Arf with target proteins, such as the GAPs. The crystal structure of non-myristoylated [L8K]Arf1•G3D extends our understanding of the N-terminus of Arf in that we find that the single residue mutation significantly changes the mechanism of binding. The association is fortuitous, but nevertheless the result provides evidence for the sequence of the N-terminus of Arf dictating specific protein-protein interfaces. The importance of the N-terminal sequence together with the recognition that the myristate might affect Arf activity by preventing off-target binding, led us to reexamine mutants that had previously been examined in the non-myristoylated Arf, this time in the context of myristoylated Arf.

By comparing mutants in the context of myristoylated Arf1 with the same mutants in non-myristoylated Arf1, we gained some insight into GAP-catalyzed conversion of Arf•GTP to Arf•GDP that might involve a cooperative effect between the N-terminal amino acids and the myristate. We previously reported that the N-terminal extensions of Arf proteins are required for efficient catalytic activity of PH domain-dependent Arf GAPs [12, 13]. Studied in ASAP1, the mechanism entails direct binding of the N-terminus of Arf to the PH domain of the GAP. Mutational analysis in the background of non-myristoylated Arf1 identified a number of critical residues within the N-terminus for Arf GAP-catalyzed GTP hydrolysis; however, little or no effect of mutating L8 or F13 was found in the context of the non-myristoylated protein [14]. In contrast, mutating F13 to alanine decreased activity almost 3000-fold when using myristoylated Arf1. By itself, mutations of L8 did not affect activity, but when mutated to alanine, reversed the effect of mutating F13. One plausible explanation of these results was that the two residues operate with the myristate to regulate alpha helical content of the N-terminal extension, presuming Arf GAPs bind the Arf N-terminus while folded as an alpha helix. However, using MD, we did not detect any effect of the mutations on secondary structure. An alternate explanation, which we are now exploring, is related to the extraction the N-terminus of Arf from the membrane to bind the PH domain of the Arf GAP, which might be a necessary step in catalysis. If L8 cooperates with myristate to anchor the N-terminus in the membrane and F13 makes contact with the GAP to extract the peptide from the membrane, one might expect mutation of F13 to reduce GAP activity consequent to an inability to extract the N-terminus of Arf from the membrane, while mutation of L8 to alanine would reduce the energy required to extract the peptide, thereby reversing the effect of mutating F13.

Spontaneous and Brag2-catalyzed myrArf1 binding to GTP did not differ between WT and the mutants we examined. The result might be expected, given that the N-terminal extension of Arf is disordered when the myristoyl moiety is present [23] and in the crystal structure of [Δ 17]Arf1•G3D in complex with Brag2_{Sec7-PH} (PDB accession code: 4C0A), the N-terminal extension is not near Brag2 [21]. Thus, our results are consistent with the prevailing hypothesis that rearrangement of the interswitch domain with subsequent accommodation of the myristate within a bilayer drive the change in the N-terminal extension on exchange of GDP for GTP. The N-terminal amino acids do not have a direct role for GEF-catalyzed nucleotide exchange other than facilitating interaction with the membrane via hydrophobic residues.

The differences between how the Arf GAPs and Arf GEFs recognize Arf is relevant to their ability to use myrArf or non-myristoylated Arf proteins as substrates in two respects. We outline hypothetical mechanistic models for how Arf GEFs and GAPs catalyze reactions using native myrArf in Fig 7. As described above, with the myristate removed, the N-terminus fills the hydrophobic cleft normally occupied by the myristate. As the N-terminal extension is disordered in a native context, this could explain why the non-myristoylated Arf1 and [L8K]Arf1 proteins are poor substrates for GEFs, as the N-terminus has multiple contacts stabilizing its association with the G domain, preventing both its removal from the cleft and the movement of the interswitch region that occurs upon GEF binding [21]. In a native context, the N-terminus of Arf is not mediating contacts with the protein and only the extraction of the myristate from the cleft and nucleotide exchange need to be catalyzed (Fig 7A). For the GAPs, the transition being catalyzed might require extraction of the N-terminus from the membrane (Fig 7B). This is further supported by our own observations that the Arf GAP ASAP1 binds via its PH domain directly to the N-terminus of Arf1 [13], as well as that the small molecule NAV-2729 inhibits PH domain-dependent Arf GAPs [25] by potentially disrupting Arf GAP:Arf N-terminal extension interactions. The differences also explain, in part, why so much has been learned about exchange factors using the truncated mutants of Arf proteins while the Arf GAPs have not been able to be studied with the truncated mutants—while the N-terminus is not necessary for exchange reactions to occur, key binding interactions with Arf GAPs are lost when the N-terminus of Arf is not present.

In summary, we provide a crystal structure of an Arf1 variant, and also observed a cooperative effect of the myristate and N-terminal extension that controls Arf GAP activity. These results provide insights into the Arf GAP catalytic mechanism. Further, we highlight the value of utilizing GTPases in their native form (or as close as possible) for *in vitro* studies designed to determine the mechanism of action of various Arf regulators or effectors.

Materials and methods

Chemicals

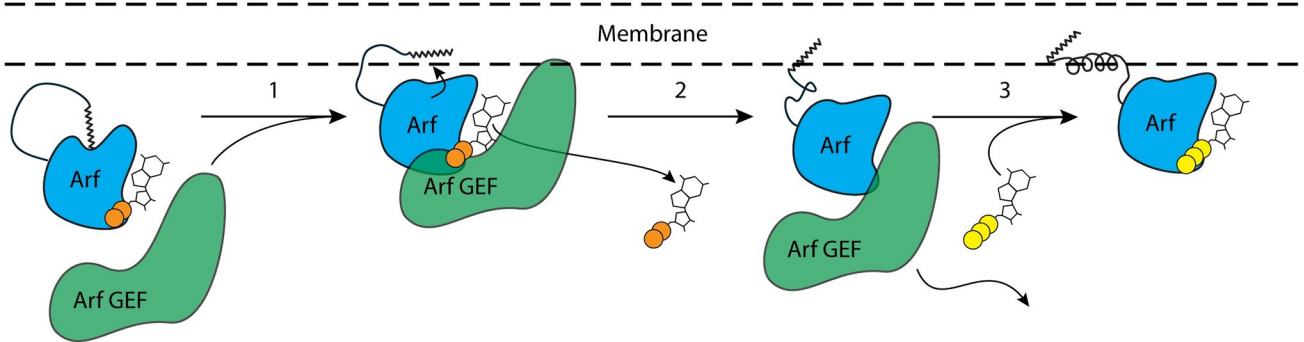
Both [α ³²P]GTP and [³⁵S]GTP γ S were obtained from Perkin-Elmer.

Protein expression and purification

Non-myristoylated [L8K]Arf1 [8], the Sec7 and PH domains (Sec7-PH construct) of Brag2 (both His-tagged for assays, and GST-tagged for myrArf1 purifications, see below) [36], the PH, Arf GAP, and ankyrin repeats (PZA construct) of ASAP1 [41], full-length AGAP1 [42], and the tandem PH domains, Arf GAP, and ankyrin repeats of ARAP1 (PPZA construct) [39] were expressed and purified as previously described.

Expression of myrArf1 proteins with C-terminal 6x His tags was accomplished via co-expression with yeast N-myristoyltransferase (yNMT) using the pETDuet-1 vector (Novagen) in *E. coli* BL-21(DE3) as previously described [43]. Expressed myrArf1 proteins were purified

A



B

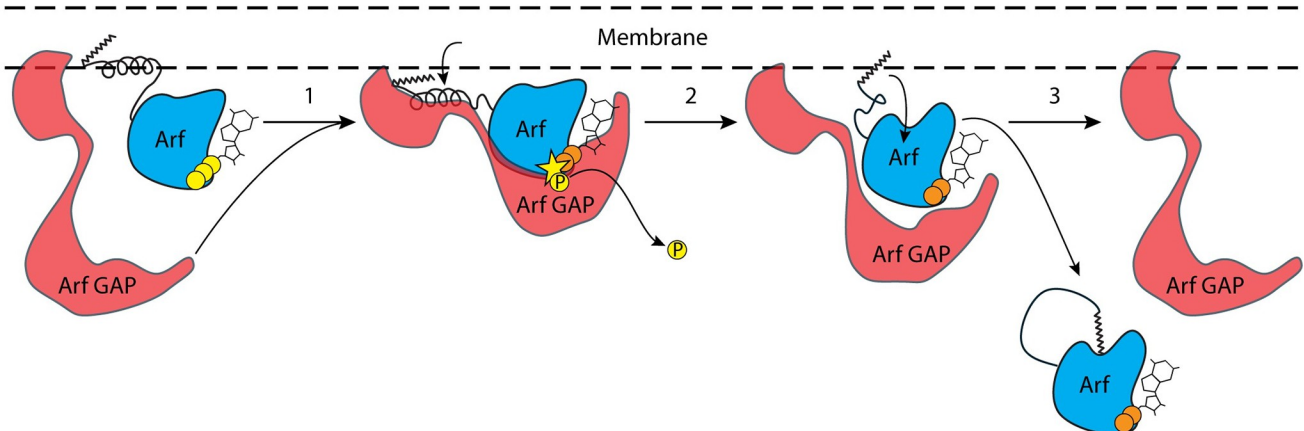


Fig 7. Theoretical mechanistic models for nucleotide and membrane cycling of myrArf proteins. (A) Mechanistic model for Arf GEF-mediated exchange of GDP for GTP. In step 1, the Arf GEF first binds to myrArf-GDP. At this stage, the N-terminal extension is disordered, and the myristate moiety is localized within the G domain hydrophobic cavity. In step 2, GDP dissociates from the G domain, which is now stabilized by the Arf GEF. Movement of the interswitch region causes the hydrophobic cavity to shrink, thereby ejecting the N-terminal extension and myristate and allowing them to associate with the membrane. In step 3, the N-terminal extension folds into an alpha helix and GTP associates with myrArf, causing the Arf GEF to dissociate. At the end of the reaction, myrArf-GTP is bound to the membrane via the N-terminal extension hydrophobic amino acids and the myristate. (B) Mechanistic model for Arf GAP-mediated degradation of GTP to GDP and inorganic phosphate. In step 1, the Arf GAP first binds to myrArf-GTP. At this stage, the N-terminal extension is associated with the membrane and myristate and is folded into an alpha helix. In step 2, interactions between the Arf GAP (e.g., through a PH domain) and the myristoylated N-terminal extension likely help to stabilize the removal of the N-terminus from the membrane. The Arf GAP also catalyzes the degradation of GTP to GDP and inorganic phosphate (the latter shown as a yellow circle with the letter "P"). Inorganic phosphate dissociates from the myrArf-GDP:Arf GAP complex. In step 3, movement of the interswitch region causes the hydrophobic cavity in the G domain to reopen, allowing the N-terminal extension to become disordered and for the myristate to enter the cavity. Finally, myrArf-GDP dissociates from the Arf GAP and the membrane.

<https://doi.org/10.1371/journal.pone.0295103.g007>

from the insoluble fraction (GTP-bound protein) following lysis and ultracentrifugation in 20 mM Tris pH 8.0, 100 mM NaCl, 1 mM MgCl₂, and 1 mM DTT (TNMD buffer) supplemented with cComplete EDTA-free protease inhibitor cocktail (Roche). The insoluble myrArf1-GTP was solubilized using 20 mM Tris pH 8.0, 100 mM NaCl, and 1 mM MgCl₂ (TNM buffer) supplemented with 1% Triton X-100, and ultracentrifuged to remove remaining insoluble material. Solubilized myrArf1-GTP was enriched via ammonium sulfate precipitation (35% at 0°C) and ultracentrifugation, whereupon it salted out as a membrane film. The supernatant was removed, and the membrane was resuspended in TNM buffer + 1% Triton X-100. The GTP-

bound myrArf1 was then converted to its GDP-bound state by addition of EDTA to 2 mM (to buffer Mg²⁺ concentrations to 1–10 μM), GDP to 10 mM, and GST-tagged Brag2_{Sec7-PH} to ~0.6 μM, and subsequent incubation for 1–2 hours at 30°C. After, the exchange reaction was quenched by addition of MgCl₂ to 2 mM. The sample was then diluted fivefold with fresh TNM, ultracentrifuged to clarify, and the soluble GDP-bound protein was loaded onto a 1 mL HisTrap HP nickel column (Cytiva) pre-equilibrated with 20 mM Tris pH 8.0, 500 mM NaCl, 20 mM imidazole (His buffer A). The myrArf1•GDP protein was washed with ≥10 column volumes (CV) of His buffer A to remove Triton X-100 and GST-Brag2_{Sec7-PH}, and was then eluted using a linear gradient of 10 CV to His buffer B (20 mM Tris pH 8.0, 500 mM NaCl, 500 mM imidazole). Eluates containing myrArf1•GDP were further purified by size exclusion chromatography (SEC) using a HiLoad 26/600 Superdex 75 prep grade column (GE Healthcare) pre-equilibrated and then run in an isocratic manner using fresh TNMD buffer at 4°C. SEC eluates of sufficient purity were pooled, concentrated using a 10,000 MWCO concentrator (Amicon), aliquoted, and snap-frozen using liquid nitrogen.

Crystallization of [L8K]Arf1•G3D and X-ray data collection and processing

Purified (≥95%) [L8K]Arf1 protein was concentrated to 10 mg/mL in TNMD buffer and was subsequently used to set crystal trays at 4°C. Initial screens were performed with the protein pre-incubated with small molecule ligands using a Mosquito system (TTP Labtech) and several commercial crystal screens from Hampton Research, Molecular Dimensions, and Emerald Bio-Systems by the hanging-drop method. The following day, ~13% of all crystal drops exhibited needle-like crystals. A tray of the *apo* protein was then set using the Mosquito system and the PEG/Ion commercial screen (Hampton Research) using a 1:1 drop ratio of protein to precipitant (250 nL each). Multiple hits were found the following day, but one of the largest needle-like crystals was in formulation #17 from the screen (0.2 M Sodium nitrate, 20% w/v Polyethylene glycol 3,350, pH 6.8). This crystal was harvested directly from the screening tray after approximately a week and a half, without cryoprotectant, and was used for data collection.

Data collection was performed at the Advanced Photon Source (APS) synchrotron beamline 22-ID with a cryostream set to 100 K. The wavelength used for data collection was 1.0 Å, and a full data set was collected to 1.75 Å resolution using a Dectris EIGER X 16M detector (see Table 1 for details of data collection). The data sets were processed using HKL-2000 [44] and the intensity data was then imported into the Phenix software suite [45] as an.mtz file. The structure of the protein was solved using Phaser [46] to perform molecular replacement with a monomer of non-myristoylated Arf1•GDP (PDB entry 1HUR) [22]. Examination of the initial molecular replacement solution in Coot [47] showed numerous obvious errors in the placements of residues within the interswitch region of the G domain, as well as the N-terminal extension. To fix these issues, the residues in these regions were removed, and then manually built in Coot using the positive F_o–F_c electron density, contoured at 3σ, as a guide. The updated coordinates containing all visible amino acid residues was then iteratively refined in Phenix and Coot (see Table 1 for details of refinement). Due to the large variations in the L8K structure compared to our search model (a 1HUR monomer, which exhibited an R_{free} of ~0.34 with our data), phase bias was not considered a significant concern. The final structure exhibited no Ramachandran outliers and ~1.2% of residues were in the allowed region.

Visualization and analysis of structural features

Structures were visualized in PyMOL (Schrödinger) [48]. RMSD calculations were made using the SuperPose web server [49]. G domain hydrophobic cavity and N-terminal extension

surface area estimates were performed in PyMOL using the “get_area” command with a dot density of 3. For the G domain hydrophobic cavity surface area estimates in non-myristoylated WT Arf1 (PDB: 1HUR), the residues I20, L37, L39, Y58, I61, F63, L166, Y167, L170, L173, S174, and L177 were selected, yielding a surface area of 1373 Å². For [L8K]Arf1, the same residues excluding Y58 were selected, yielding a surface area of 1243 Å², or a reduction in area compared to non-myristoylated WT of ~10%. For N-terminal extension surface area estimates in the non-myristoylated WT Arf1 structure, the residues G2, I4, F5, A6, L8, F9, L12, and M18 of a monomer were selected, yielding a surface area of 849 Å². For [L8K]Arf1, the residues K8, F9, K10, L12, F13, and M18 were selected, yielding a surface area of 754 Å², or a reduction in contact area compared to non-myristoylated WT of ~11%; if K10 is excluded from the analysis, the surface area and percent reduction in contact area are instead 628 Å² and 26%.

Cloning of Arf1 mutants

The Arf1 mutants L8K, L8A, F13A, and L8A/F13A were generated by site-directed mutagenesis of the Arf1/yNMT in pETDuet-1 plasmid described above as a template. Briefly, reactions were performed with mutagenesis primers and the Q5 DNA polymerase (New England Biolabs). Afterward, the template DNA was digested using *DpnI* enzyme (New England Biolabs). Mutagenized DNA was transformed into NEB® 5-alpha competent *E. coli* (New England Biolabs), and individual colonies were cultured, used to generate miniprepped DNA with a commercial kit (Qiagen), and sequenced with pET Upstream primer (Novagen). Sequencing was conducted at the Center for Cancer Research (CCR) Genomics Core at the National Cancer Institute, Bethesda, MD. Plasmid DNA with the correct sequences were then transformed into BL-21(DE3) *E. coli* for large-scale expression.

Preparation of LUVs

LUVs were prepared by extrusion. Briefly, 1 μmol lipids, dissolved in chloroform in a siliconized glass tube, with molar ratio of 40% phosphatidylcholine, 25% phosphatidylethanolamine, 15% phosphatidylserine, 10% cholesterol, and 10% total phosphoinositide (2.5% phosphatidylinositol 4,5-bisphosphate [PIP2], 0.5% phosphatidylinositol (3,4,5)-trisphosphate, and 7% phosphatidylinositol [PI] for ARAP1 GAP activity, 1% PIP2 and 9% PI for all other experiments) were dried under a nitrogen stream for 30 minutes to 1 hour, followed by lyophilization for at least one hour. The dried lipids were resuspended in 200 μL 1x PBS, for a final concentration of 5 mM. The solution was vortexed, subjected to five rounds of freeze/thaw, and extruded using a lipid extruder (Avanti Polar Lipids) through a Whatman Nuclepore Track-Etched membrane with 1 μM pores. The LUVs were stored at 4°C and were used within a week for activity assays.

Spontaneous guanine nucleotide exchange assays

Spontaneous exchange assays were performed as previously described [7, 12]. Exchange reaction mixtures contained 25 mM HEPES, pH 7.4, 100 mM NaCl, 1 mM dithiothreitol, 0.5 mM MgCl₂, 1 mM EDTA, 5 μM GTPγS spiked with [³⁵S]GTPγS, 0.5 mM LUVs, and 0.5 μM myr-Arf1•GDP. The reactions were incubated at 30°C for indicated periods of time and then quenched with 2 mL of ice-cold 20 mM Tris, pH 8.0, 100 mM NaCl, 10 mM MgCl₂, and 1 mM dithiothreitol. Protein-bound nucleotide was trapped on nitrocellulose, and the bound radioactivity was quantified by liquid scintillation counting. Data were plotted in GraphPad Prism and fit to a one-phase association model.

GEF activity assays

GEF activity assays were performed as previously described [36]. Reaction mixtures contained 25 mM HEPES, pH 7.4, 100 mM NaCl, 1 mM dithiothreitol, 2 mM MgCl₂, 1 mM EDTA, 5 μM GTPγS spiked with [³⁵S]GTPγS, 0.5 mM LUVs, 0.5 μM myrArf1•GDP, and variable concentrations of Brag2_{Sec7-PH}. The reactions were incubated at 30°C for 3 min. and quenched with 2 mL of ice-cold 20 mM Tris, pH 8.0, 100 mM NaCl, 10 mM MgCl₂, and 1 mM dithiothreitol. Protein-bound nucleotide was trapped on nitrocellulose, and the bound radioactivity was quantified by liquid scintillation counting. Data were plotted in GraphPad Prism and fit to a one site specific binding model.

GTP hydrolysis and GAP activity assays

GAP-induced conversion of myrArf1•GTP to myrArf1•GDP was determined as described previously [13, 50]. Reaction mixtures contained 25 mM HEPES, pH 7.4, 100 mM NaCl, 1 mM dithiothreitol, 2 mM MgCl₂, 1 mM GTP, 0.5 mM LUVs, myrArf1 bound to [$\alpha^{32}\text{P}$]GTP, and variable concentrations of Arf GAP. The LUVs were included in the myrArf1 GTP loading reaction. The reactions were incubated at 30°C for 3 minutes (unless otherwise specified), and quenched with 2 mL of ice-cold 20 mM Tris, pH 8.0, 100 mM NaCl, 10 mM MgCl₂, and 1 mM dithiothreitol. Protein-bound nucleotide was trapped on nitrocellulose, and guanine nucleotide was released by addition of formic acid. [$\alpha^{32}\text{P}$]GDP and [$\alpha^{32}\text{P}$]GTP were then separated using thin-layer chromatography plates, and quantified. Data were plotted in GraphPad Prism and fit to a one site specific binding model.

Molecular dynamics simulations

We modelled the amphipathic helix (residues 2–17) of myr-Arf1, including the N-terminal myristoyl group in a membrane bilayer. Five simulations were performed including WT myr-Arf1 and mutations L8K, L8A, F13A and L8A/F13A. The system was built in the CHARMM-GUI membrane builder. Each bilayer contained two of the amphipathic helices evenly distributed in each monolayer, 9 Å above the center of the bilayer. All equilibration and MD simulations were performed using AMBER with the CHARMM force field and solvated by TIP3P water molecules. The membrane contained 150 lipids in each monolayer with 142 (DMPC) and 8 PI(4,5)P₂ lipids. The system was solvated with ~15,000 TIP3 water molecules. Each simulation contained 40 Cl[−] ions and 100 K⁺ ions with the exception of L8K, which included 96 K⁺ ions. The simulation box had dimensions measuring 129 Å × 129 Å × 70 Å. The system was equilibrated for six steps (steps 1–3 for 125 ps and 4–6 for 500 ps). Simulations were then performed for 1.5–2.5 μs at 303.15 K. Details of simulations are shown in Table 4.

Orientation and depth of insertion from MD structures

The tilt of each peptide was obtained by calculating the angle between the smallest moment of inertia of the alpha helical segment and the membrane surface. The tilt angle is equal to zero

Table 4. Statistics of molecular dynamics simulations of myrArf1 N-terminal extensions.

	Total # of atoms	# of TIP3 water	# of μs
WT	82324	15056	2.29
L8K	82408	15092	1.78
L8A	82204	15028	1.79
F13A	82422	15102	2.49
L8A/F13A	82323	15081	2.48

<https://doi.org/10.1371/journal.pone.0295103.t004>

when the axis of the smallest moment of inertia is parallel to the membrane surface and negative when the N-terminus is lower than the C-terminus on the z axis (membrane normal). The depth of insertion of a peptide was calculated as the distance between the center of mass for heavy backbone atoms and the center of the bilayer.

Supporting information

S1 Text. Discussion regarding the decreased apparent maximum GTP hydrolysis observed with [L8A/F13A]myrArf1.

(DOCX)

S1 Fig. Detailed analyses of [L8K]Arf1•G3D crystal structure. (A) Polder OMIT map [51] of the atoms composing guanosine-3'-monophosphate-5'-diphosphate (G3D) within the [L8K]Arf1•G3D crystal structure. Green and red mesh corresponds to positive and negative $mF_{\text{obs}} - DF_{\text{model}}$ OMIT difference density contoured at 3σ . (B) Interswitch region crystal contacts between monomers within the [L8K]Arf1•G3D crystal structure. The interswitch region of one monomer (pink) is adjacent to an alpha helix between the P-loop and switch I in the G domain of another monomer (green). Crystal contact regions are emphasized with yellow dashed lines, and distances in Angstroms are shown. N-terminus and contact residues are labeled, and the L8K mutation is shown in yellow. (C) G5 motif crystal contacts between monomers within the [L8K]Arf1•G3D crystal structure. The G5 motif of one monomer (pink) is adjacent to an alpha helix towards the C-terminal end of the G domain of another monomer (green). Residues and crystal contacts are emphasized as in (B). Note that the L8K mutation residue (yellow) is near D141 in this same symmetry mate. (D) Hinge regions between N-terminal extension and G domains in Arf1 structures. The coloring of each structure is consistent with the colors used in Fig 1. The backbone atoms of K16 are shown in yellow and labeled, and the distances between K16 α -carbons are shown in yellow dashed lines. Distances are in Angstroms.

(TIF)

S2 Fig. Spontaneous guanine nucleotide exchange of myrArf1 constructs. For these assays, 0.5 μM myrArf1 constructs was added to a reaction with low (1–10 μM) Mg^{2+} to promote exchange, as well as [^{35}S]GTP γ S and LUVs. After the indicated period of time, the fraction of myrArf1 bound to [^{35}S]GTP γ S was measured. Data shown are a representative example from multiple experiments.

(TIF)

S3 Fig. Kinetic analyses of GTP hydrolysis using indicated myrArf1•GTP. (A) Time course of Arf GAP activity with high concentrations (5 nM) of ASAP1_{PZA} using WT or [L8A/F13A] myrArf1•GTP as substrates. For these assays, myrArf1 was loaded with [$\alpha^{32}\text{P}$]GTP, ASAP1_{PZA} was added, the reaction was quenched after the indicated incubation time, and the ratio of [$\alpha^{32}\text{P}$]GDP and [$\alpha^{32}\text{P}$]GTP bound to myrArf1 was measured. Data shown are a representative example from multiple experiments. (B) Time course of spontaneous GTP hydrolysis on myrArf1 constructs. For these assays, myrArf1 was loaded with [$\alpha^{32}\text{P}$]GTP for 30 minutes. Following the indicated periods of time after addition of GAP reaction buffer containing Mg^{2+} and GTP, the reaction was quenched and the ratio of [$\alpha^{32}\text{P}$]GDP and [$\alpha^{32}\text{P}$]GTP bound to myrArf1 was measured. The panel on top shows the change in GTP hydrolyzed compared to that at time 0 minutes (immediately after 30 minutes of GTP loading then quenching); the panel on bottom is the same data, showing the full ratio of measured GTP over the sum of measured GDP and GTP. Data shown are a representative example from multiple experiments.

(TIF)

S4 Fig. Detailed statistics of myrArf1 N-terminal peptide interaction with membrane from MD simulations. (A) Per residue roll angle for WT myrArf1 peptide and its mutants. WT myrArf1 per residue roll angles are compared to [L8A]myrArf1, [F13A]myrArf1, and [L8A/F13A]myrArf1 (top) or [L8K]myrArf1 (bottom). Roll angles are calculated as the angle between the C^{α} - H^{α} bond of a residue and the bilayer normal. An angle of 0° corresponds to the C^{α} - H^{α} bond aligned with the bilayer normal and pointing toward the hydrophobic core of the membrane. (B) Insertion depth (left) and average orientation (right) relative to the monolayer phosphate membrane plane of [L8K]myrArf1 N-terminal peptide. A tilt angle of zero means that the helical axis is parallel to the membrane surface. A negative tilt angle means the peptide is tilted such that the N-terminus is lower than the C-terminus on the z-axis (membrane normal).

(TIF)

S1 File.

(PDF)

Acknowledgments

We would also like to thank Drs. Richard A. Kahn and David Lambright for their insights into the molecule G3D.

Author Contributions

Conceptualization: Eric M. Rosenberg, Jr., Xiaoying Jian, Olivier Soubias, Paul A. Randazzo.

Data curation: Eric M. Rosenberg, Jr., Xiaoying Jian, Olivier Soubias.

Formal analysis: Eric M. Rosenberg, Jr., Xiaoying Jian, Olivier Soubias, Lothar Esser, Alexander J. Sodt, Di Xia.

Funding acquisition: Paul A. Randazzo.

Investigation: Eric M. Rosenberg, Jr., Xiaoying Jian, Olivier Soubias, Rebekah A. Jackson, Erin Gladu, Emily Andersen, Lothar Esser, Alexander J. Sodt, Di Xia.

Methodology: Eric M. Rosenberg, Jr.

Project administration: Paul A. Randazzo.

Supervision: Di Xia, R. Andrew Byrd.

Visualization: Eric M. Rosenberg, Jr., Xiaoying Jian.

Writing – original draft: Eric M. Rosenberg, Jr., Paul A. Randazzo.

Writing – review & editing: Eric M. Rosenberg, Jr., Xiaoying Jian, Olivier Soubias, Lothar Esser, Alexander J. Sodt, R. Andrew Byrd.

References

1. Donaldson JG, Jackson CL. ARF family G proteins and their regulators: roles in membrane transport, development and disease. *Nature reviews Molecular cell biology*. 2011; 12(6):362–75. Epub 2011/05/19. <https://doi.org/10.1038/nrm3117> PMID: 21587297; PubMed Central PMCID: PMC3245550.
2. D'Souza-Schorey C, Chavrier P. ARF proteins: roles in membrane traffic and beyond. *Nature reviews Molecular cell biology*. 2006; 7(5):347–58. Epub 2006/04/25. <https://doi.org/10.1038/nrm1910> PMID: 16633337.

3. Kahn RA, Gilman AG. The protein cofactor necessary for ADP-ribosylation of Gs by cholera toxin is itself a GTP binding protein. *J Biol Chem.* 1986; 261(17):7906–11. Epub 1986/06/15. PMID: [3086320](#).
4. East MP, Kahn RA. Models for the functions of Arf GAPs. *Seminars in cell & developmental biology.* 2011; 22(1):3–9. Epub 2010/07/20. <https://doi.org/10.1016/j.semcd.2010.07.002> PMID: [20637885](#); PubMed Central PMCID: [PMC2976832](#).
5. Paduch M, Jeleń F, Otlewski J. Structure of small G proteins and their regulators. *Acta biochimica Polonica.* 2001; 48(4):829–50. Epub 2002/05/09. PMID: [11995995](#).
6. Peurois F, Peyroche G, Cherfils J. Small GTPase peripheral binding to membranes: molecular determinants and supramolecular organization. *Biochemical Society Transactions.* 2018; 47(1):13–22. <https://doi.org/10.1042/BST20170525> PMID: [30559268](#)
7. Randazzo PA, Terui T, Sturch S, Fales HM, Ferrige AG, Kahn RA. The myristoylated amino terminus of ADP-ribosylation factor 1 is a phospholipid- and GTP-sensitive switch. *J Biol Chem.* 1995; 270(24):14809–15. Epub 1995/06/16. <https://doi.org/10.1074/jbc.270.24.14809> PMID: [7782347](#).
8. Kahn RA, Randazzo P, Serafini T, Weiss O, Rulka C, Clark J, et al. The amino terminus of ADP-ribosylation factor (ARF) is a critical determinant of ARF activities and is a potent and specific inhibitor of protein transport. *J Biol Chem.* 1992; 267(18):13039–46. Epub 1992/06/25. PMID: [1618801](#).
9. Kahn RA, Clark J, Rulka C, Stearns T, Zhang CJ, Randazzo PA, et al. Mutational analysis of *Saccharomyces cerevisiae* ARF1. *J Biol Chem.* 1995; 270(1):143–50. Epub 1995/01/06. <https://doi.org/10.1074/jbc.270.1.143> PMID: [7814365](#).
10. Plowman SJ, Hancock JF. Ras signaling from plasma membrane and endomembrane microdomains. *Biochimica et biophysica acta.* 2005; 1746(3):274–83. Epub 2005/07/26. <https://doi.org/10.1016/j.bbamcr.2005.06.004> PMID: [16039730](#).
11. Giglione C, Meinnel T. Mapping the myristoylome through a complete understanding of protein myristylation biochemistry. *Progress in lipid research.* 2022; 85:101139. Epub 2021/11/19. <https://doi.org/10.1016/j.plipres.2021.101139> PMID: [34793862](#).
12. Randazzo PA, Terui T, Sturch S, Kahn RA. The amino terminus of ADP-ribosylation factor (ARF) 1 is essential for interaction with Gs and ARF GTPase-activating protein. *J Biol Chem.* 1994; 269(47):29490–4. Epub 1994/11/25. PMID: [7961931](#).
13. Roy NS, Jian X, Soubias O, Zhai P, Hall JR, Dagher JN, et al. Interaction of the N terminus of ADP-ribosylation factor with the PH domain of the GTPase-activating protein ASAP1 requires phosphatidylinositol 4,5-bisphosphate. *J Biol Chem.* 2019; 294(46):17354–70. Epub 2019/10/06. <https://doi.org/10.1074/jbc.RA119.009269> PMID: [31591270](#).
14. Yoon HY, Jacques K, Nealon B, Stauffer S, Premont RT, Randazzo PA. Differences between AGAP1, ASAP1 and Arf GAP1 in substrate recognition: interaction with the N-terminus of Arf1. *Cellular signaling.* 2004; 16(9):1033–44. Epub 2004/06/24. <https://doi.org/10.1016/j.cellsig.2004.02.008> PMID: [15212764](#).
15. Andreev J, Simon JP, Sabatini DD, Kam J, Plowman G, Randazzo PA, et al. Identification of a new Pyk2 target protein with Arf-GAP activity. *Mol Cell Biol.* 1999; 19(3):2338–50. Epub 1999/02/18. <https://doi.org/10.1128/MCB.19.3.2338> PMID: [10022920](#); PubMed Central PMCID: [PMC84026](#).
16. Ding M, Vitale N, Tsai SC, Adamik R, Moss J, Vaughan M. Characterization of a GTPase-activating protein that stimulates GTP hydrolysis by both ADP-ribosylation factor (ARF) and ARF-like proteins. Comparison to the ARD1 gap domain. *J Biol Chem.* 1996; 271(39):24005–9. Epub 1996/09/27. <https://doi.org/10.1074/jbc.271.39.24005> PMID: [8798635](#).
17. Liu Y, Kahn RA, Prestegard JH. Dynamic structure of membrane-anchored Arf*GTP. *Nature structural & molecular biology.* 2010; 17(7):876–81. Epub 2010/07/06. <https://doi.org/10.1038/nsmb.1853> PMID: [20601958](#); PubMed Central PMCID: [PMC2921649](#).
18. Paris S, Béraud-Dufour S, Robineau S, Bigay J, Antonny B, Chabre M, et al. Role of Protein-Phospholipid Interactions in the Activation of ARF1 by the Guanine Nucleotide Exchange Factor Arno*. *Journal of Biological Chemistry.* 1997; 272(35):22221–6. <https://doi.org/10.1074/jbc.272.35.22221> PMID: [9268368](#)
19. Béraud-Dufour S, Paris S, Chabre M, Antonny B. Dual interaction of ADP ribosylation factor 1 with Sec7 domain and with lipid membranes during catalysis of guanine nucleotide exchange. *J Biol Chem.* 1999; 274(53):37629–36. Epub 1999/12/23. <https://doi.org/10.1074/jbc.274.53.37629> PMID: [10608818](#).
20. Randazzo PA, Nie Z, Hirsch DS. Arf and Phospholipids. In: Kahn RA, editor. *ARF Family GTPases.* Dordrecht: Springer Netherlands; 2003. p. 49–69.
21. Aizel K, Biou V, Navaza J, Duarte LV, Campanacci V, Cherfils J, et al. Integrated conformational and lipid-sensing regulation of endosomal ArfGEF BRAG2. *PLoS biology.* 2013; 11(9):e1001652. Epub 2013/09/24. <https://doi.org/10.1371/journal.pbio.1001652> PMID: [24058294](#); PubMed Central PMCID: [PMC3769224](#).

22. Amor JC, Harrison DH, Kahn RA, Ringe D. Structure of the human ADP-ribosylation factor 1 complexed with GDP. *Nature*. 1994; 372(6507):704–8. Epub 1994/12/15. <https://doi.org/10.1038/372704a0> PMID: 7990966.
23. Liu Y, Kahn RA, Prestegard JH. Structure and membrane interaction of myristoylated ARF1. Structure (London, England: 1993). 2009; 17(1):79–87. Epub 2009/01/15. <https://doi.org/10.1016/j.str.2008.10.020> PMID: 19141284; PubMed Central PMCID: PMC2659477.
24. Che MM, Boja ES, Yoon H-Y, Gruschus J, Jaffe H, Stauffer S, et al. Regulation of ASAP1 by phospholipids is dependent on the interface between the PH and Arf GAP domains. *Cellular signalling*. 2005; 17(10):1276–88. <https://doi.org/10.1016/j.cellsig.2005.01.007> PMID: 16038802
25. Rosenberg EM Jr, Jian X, Soubias O, Yoon HY, Yadav MP, Hammoudeh S, et al. The small molecule inhibitor NAV-2729 has a complex target profile including multiple ADP-ribosylation factor regulatory proteins. *J Biol Chem*. 2023; 299(3):102992. Epub 2023/02/10. <https://doi.org/10.1016/j.jbc.2023.102992> PMID: 36758799; PubMed Central PMCID: PMC10023970.
26. Amor JC, Horton JR, Zhu X, Wang Y, Sullards C, Ringe D, et al. Structures of yeast ARF2 and ARL1: distinct roles for the N terminus in the structure and function of ARF family GTPases. *J Biol Chem*. 2001; 276(45):42477–84. Epub 2001/09/06. <https://doi.org/10.1074/jbc.M106660200> PMID: 11535602.
27. Renault L, Guibert B, Cherfils J. Structural snapshots of the mechanism and inhibition of a guanine nucleotide exchange factor. *Nature*. 2003; 426(6966):525–30. Epub 2003/12/05. <https://doi.org/10.1038/nature02197> PMID: 14654833.
28. Stogios PJ, Michalska K, Evdokimova E., Di Leo, Savchenko R, Joachimiak A, A., et al. Center for Structural Genomics of Infectious Diseases (CSGID). Crystal structure of ARF3 from *Candida albicans* in complex with guanosine-3'-monophosphate-5'-diphosphate. 2021. <https://doi.org/10.2210/pdb7rl/pdb>.
29. Wang ZX, Shi L, Liu JF, An XM, Chang WR, Liang DC. 2.0 A crystal structure of human ARL5-GDP3'P, a novel member of the small GTP-binding proteins. *Biochemical and biophysical research communications*. 2005; 332(3):640–5. Epub 2005/05/18. <https://doi.org/10.1016/j.bbrc.2005.04.168> PMID: 15896705.
30. Crystal Structure of Rab28A GTPase in the Inactive (GDP-3'P-Bound) Form [Internet]. 2007.
31. Crystal Structure of YorR protein in complex with phosphorylated GDP from *Bacillus subtilis*, Northeast Structural Genomics Consortium Target SR256 [Internet]. 2009.
32. Pao CC, Gallant J. A new nucleotide involved in the stringent response in *Escherichia coli*. Guanosine 5'-diphosphate-3'-monophosphate. *J Biol Chem*. 1979; 254(3):688–92. 368059.
33. Pao CC, Dyess BT. Effect of unusual guanosine nucleotides on the activities of some *Escherichia coli* cellular enzymes. *Biochimica et biophysica acta*. 1981; 677(3–4):358–62. [https://doi.org/10.1016/0304-4165\(81\)90247-6](https://doi.org/10.1016/0304-4165(81)90247-6) PMID: 6117328.
34. Crosse AM, Greenway DL, England RR. Accumulation of ppGpp and ppGp in *Staphylococcus aureus* 8325–4 following nutrient starvation. *Lett Appl Microbiol*. 2000; 31(4):332–7. <https://doi.org/10.1046/j.1472-765x.2000.00822.x> PMID: 11068918.
35. Zhang Y, Soubias O, Pant S, Heinrich F, Vogel A, Li J, et al. Myr-Arf1 conformational flexibility at the membrane surface sheds light on the interactions with ArfGAP ASAP1. *Nature communications*. 2023; 14(1):7570. Epub 2023/11/21. <https://doi.org/10.1038/s41467-023-43008-5> PMID: 37989735; PubMed Central PMCID: PMC10663523.
36. Jian X, Gruschus JM, Sztul E, Randazzo PA. The pleckstrin homology (PH) domain of the Arf exchange factor Brag2 is an allosteric binding site. *J Biol Chem*. 2012; 287(29):24273–83. Epub 2012/05/23. <https://doi.org/10.1074/jbc.M112.368084> PMID: 22613714; PubMed Central PMCID: PMC3397853.
37. Neu HC. The 5'-nucleotidase of *Escherichia coli*. I. Purification and properties. *J Biol Chem*. 1967; 242(17):3896–904. Epub 1967/09/10. PMID: 5341265.
38. Nie Z, Stanley KT, Stauffer S, Jacques KM, Hirsch DS, Takei J, et al. AGAP1, an endosome-associated, phosphoinositide-dependent ADP-ribosylation factor GTPase-activating protein that affects actin cytoskeleton. *J Biol Chem*. 2002; 277(50):48965–75. Epub 2002/10/22. <https://doi.org/10.1074/jbc.M202969200> PMID: 12388557.
39. Campa F, Yoon HY, Ha VL, Szentpeteri Z, Balla T, Randazzo PA. A PH domain in the Arf GTPase-activating protein (GAP) ARAP1 binds phosphatidylinositol 3,4,5-trisphosphate and regulates Arf GAP activity independently of recruitment to the plasma membranes. *J Biol Chem*. 2009; 284(41):28069–83. Epub 2009/08/12. <https://doi.org/10.1074/jbc.M109.028266> PMID: 19666464; PubMed Central PMCID: PMC2788858.
40. Vögler O, Barceló JM, Ribas C, Escribá PV. Membrane interactions of G proteins and other related proteins. *Biochimica et Biophysica Acta (BBA)—Biomembranes*. 2008; 1778(7):1640–52. <https://doi.org/10.1016/j.bbamem.2008.03.008> PMID: 18402765

41. Brown MT, Andrade J, Radhakrishna H, Donaldson JG, Cooper JA, Randazzo PA. ASAP1, a phospholipid-dependent arf GTPase-activating protein that associates with and is phosphorylated by Src. *Mol Cell Biol*. 1998; 18(12):7038–51. <https://doi.org/10.1128/MCB.18.12.7038> PMID: 9819391.
42. Che MM, Nie Z, Randazzo PA. Assays and properties of the Arf GAPs AGAP1, ASAP1, and Arf GAP1. *Methods in enzymology*. 2005; 404:147–63. Epub 2006/01/18. [https://doi.org/10.1016/S0076-6879\(05\)04015-2](https://doi.org/10.1016/S0076-6879(05)04015-2) PMID: 16413266.
43. Li Y, Soubias O, Li J, Sun S, Randazzo PA, Byrd RA. Functional Expression and Characterization of Human Myristoylated-Arf1 in Nanodisc Membrane Mimetics. *Biochemistry*. 2019; 58(10):1423–31. Epub 2019/02/09. <https://doi.org/10.1021/acs.biochem.8b01323> PMID: 30735034; PubMed Central PMCID: PMC7448547.
44. Otwinowski Z, Minor W. [20] Processing of X-ray diffraction data collected in oscillation mode. *Methods in enzymology*. 276: Academic Press; 1997. p. 307–26.
45. Liebschner D, Afonine PV, Baker ML, Bunkóczki G, Chen VB, Croll TI, et al. Macromolecular structure determination using X-rays, neutrons and electrons: recent developments in Phenix. *Acta crystallographica Section D, Structural biology*. 2019; 75(Pt 10):861–77. Epub 2019/10/08. <https://doi.org/10.1107/S2059798319011471> PMID: 31588918; PubMed Central PMCID: PMC6778852.
46. McCoy AJ, Grosse-Kunstleve RW, Adams PD, Winn MD, Storoni LC, Read RJ. Phaser crystallographic software. *Journal of applied crystallography*. 2007; 40(Pt 4):658–74. Epub 2007/08/01. <https://doi.org/10.1107/S0021889807021206> PMID: 19461840; PubMed Central PMCID: PMC2483472.
47. Emsley P, Lohkamp B, Scott WG, Cowtan K. Features and development of Coot. *Acta crystallographica Section D, Biological crystallography*. 2010; 66(Pt 4):486–501. Epub 2010/04/13. <https://doi.org/10.1107/S0907444910007493> PMID: 20383002; PubMed Central PMCID: PMC2852313.
48. Schrodinger LLC. The PyMOL Molecular Graphics System, Version 1.8. 2015.
49. Maiti R, Van Domselaar GH, Zhang H, Wishart DS. SuperPose: a simple server for sophisticated structural superposition. *Nucleic Acids Res*. 2004; 32(Web Server issue):W590–4. Epub 2004/06/25. <https://doi.org/10.1093/nar/gkh477> PMID: 15215457; PubMed Central PMCID: PMC441615.
50. Jian X, Tang WK, Zhai P, Roy NS, Luo R, Gruschus JM, et al. Molecular Basis for Cooperative Binding of Anionic Phospholipids to the PH Domain of the Arf GAP ASAP1. *Structure* (London, England: 1993). 2015; 23(11):1977–88. Epub 2015/09/15. <https://doi.org/10.1016/j.str.2015.08.008> PMID: 26365802; PubMed Central PMCID: PMC4788500.
51. Liebschner D, Afonine PV, Moriarty NW, Poon BK, Sobolev OV, Terwilliger TC, et al. Polder maps: improving OMIT maps by excluding bulk solvent. *Acta crystallographica Section D, Structural biology*. 2017; 73(Pt 2):148–57. Epub 2017/02/09. <https://doi.org/10.1107/S2059798316018210> PMID: 28177311; PubMed Central PMCID: PMC5297918.